Review

Advances in Strategic Inhibition of Polysulfide Shuttle in Room-Temperature Sodium-Sulfur Batteries via Electrode and Interface Engineering

Anupriya K. Haridas [1] and Chun Huang [2,3,4,*]

1 Department of Engineering, King's College London, London WC2R 2LS, UK
2 Department of Materials, Imperial College London, London SW7 2AZ, UK
3 The Faraday Institution, Quad One, Becquerel Ave, Harwell Campus, Didcot OX11 0RA, UK
4 Research Complex at Harwell, Rutherford Appleton Laboratory, Didcot OX11 0FA, UK
* Correspondence: a.huang@imperial.ac.uk

Abstract: Room-temperature sodium-sulfur batteries (RT-NaSBs) with high theoretical energy density and low cost are ideal candidates for next-generation stationary and large-scale energy storage. However, the dissolution of sodium polysulfide (NaPS) intermediates and their migration to the anode side give rise to the shuttle phenomenon that impedes the reaction kinetics leading to rapid capacity decay, poor coulombic efficiency, and severe loss of active material. Inhibiting the generation of long-chain NaPS or facilitating their adsorption via physical and chemical polysulfide trapping mechanisms is vital to enhancing the electrochemical performance of RT-NaSBs. This review provides a brief account of the polysulfide inhibition strategies employed in RT-NaSBs via physical and chemical adsorption processes via the electrode and interfacial engineering. Specifically, the sulfur immobilization and polysulfide trapping achieved by electrode engineering strategies and the interfacial engineering of the separator, functional interlayer, and electrolytes are discussed in detail in light of recent advances in RT-NaSBs. Additionally, the benefits of engineering the highly reactive Na anode interface in improving the stability of RT-NaSBs are also elucidated. Lastly, the future perspectives on designing high-performance RT-NaSBs for practical applications are briefly outlined.

Keywords: room-temperature sodium-sulfur batteries; high energy density; polysulfide shuttle; polysulfide trapping; physical and chemical strategies

1. Introduction

Energy storage has recently become a hot topic of research due to the fast depletion of non-renewable energy resources coupled with the unprecedented surge in energy demands [1,2]. With that, harvesting energy from intermittent energy sources has become quintessential to ensuring an uninterrupted power supply to the grid. Realizing efficient energy storage systems (ESS) for stationary and grid-level storage necessitates reliable and efficient high-energy battery systems with long cycle life and low cost [3]. The enormous commercial success of lithium-ion batteries (LIBs) has paved the way for compact and clean energy storage powering portable electronic devices and EVs [4]. However, the overexploitation of the limited lithium and cobalt resources has severely impeded their large-scale applications due to the exponential rise in production costs every year [5]. In such a context, next-generation battery technologies which explore low-cost raw materials are highly desirable for realizing efficient ESS in the future. Sodium (Na) with a relatively similar redox potential (-2.7 V vs. S.H.E) to that of Li (-3.0 V vs. S.H.E) and an exceptionally high geographical abundance (23,600 mg kg^{-1} vs. 20 mg kg^{-1} for Li) is undoubtedly the promising alternative for lithium in order to realize affordable and low-cost batteries [1,2,6].

The recent developments in next-generation energy storage devices, such as lithium-sulfur batteries (LSBs), have garnered tremendous attention worldwide due to the high

theoretical capacity (1675 mAh g^{-1}) and energy density (2600 Wh k g^{-1}) offered by sulfur (S) cathodes [7,8]. The two-electron transfer reaction (S^0 to S^{2-}) in LSBs results in high capacity, which accounts for almost 10 times the capacity of the commercialized LIB cathodes, making them highly desirable for ESS [9–11]. Apart from that, S is widely abundant in the Earth's crust and environmentally benign [12]. Coupling the benefits of the high energy density S cathode with the abundant and low-cost raw materials, S and Na, room temperature sodium-sulfur batteries (RT-NaSBs) are promising candidates for next-generation energy storage [13,14]. The rise in the number of publications over the past decade shows that the RT-NaSB research has regained momentum (Figure 1a). The superior theoretical energy density (Figure 1b) and the reduction in cost per kWh of RT-NaSBs (Figure 1c) compared to that of LSBs, and LIBs are apparent reasons for such a rampant research interest (Figure 1c,d) [10,15].
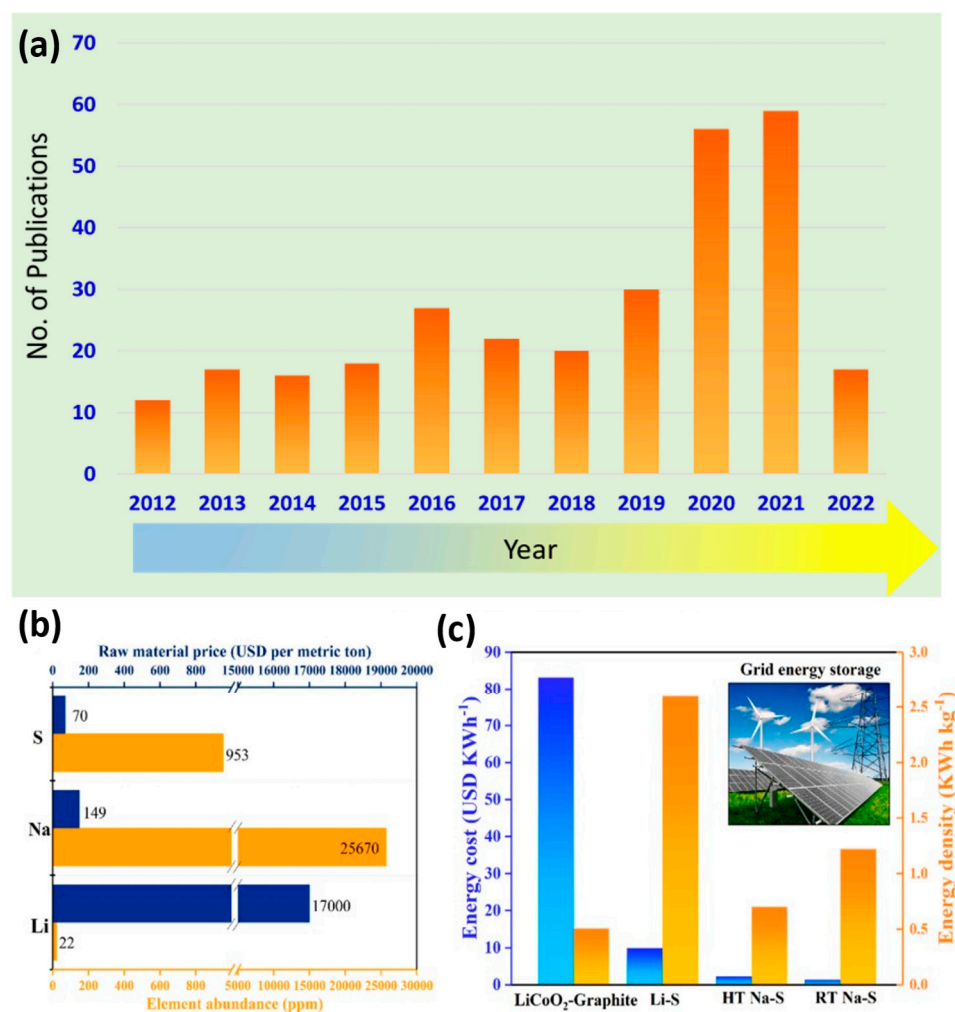

Figure 1. (**a**) Rise in the number of publications on RT-NaSBs in the last 10 years (2012–2022 March, data collected from Scopus) and comparison of (**b**) element abundance and raw material price and (**c**) projected reduction in cost per kWh in terms of energy density achieved for RT-NaSBs compared to that of prominent rechargeable battery technologies. Reproduced with permission [15]. Copyright 2021, American Chemical Society.

Despite the excellent prospects of achieving superior electrochemical performances at low cost, poor conductivity, and massive volume changes, the polysulfide shuttle phenomenon and Na dendritic growth limit the utility of RT-NaSBs. Among them, the polysulfide shuttle mechanism is a major phenomenon that requires immediate attention. Polysulfide shuttling in RT-NaSBs involve the shuttling of the soluble NaPS species from

the cathode to the anode and their unwarranted reduction at the sodium anode. This leads to low active material utilization and capacity fading in cells affecting cyclability and efficiency. It is critical to understand the reaction mechanism of polysulfide shuttling and design effective strategies to mitigate this problem so that the reversibility and cyclability of RT-NaSBs can be improved substantially.

Henceforth, this review attempts to elucidate the strategic advances in polysulfide inhibition by both electrode and interfacial engineering in view of the S cathodes, separators, electrolytes, and the Na anode. A comprehensive overview of research strategies for high-performance RT-Na-S batteries with extended cyclability is also outlined.

2. State-of-the-Art RT-NaSBs: Reaction Mechanism and Polysulfide Shuttle

The electrochemical energy storage with sodium-sulfur battery chemistry dates back to the 1960s when it was proposed for the first time to support stationary energy-storage systems [16]. Initial NaSBs consisted of molten Na electrodes and a sodium β alumina electrolyte operated at a high temperature (>300 °C) with a theoretical energy density of 760 Wh kg^{-1} based on the total mass of sodium and sulfur [17]. However, the utilization of corrosive molten electrodes and the ceramic electrolyte at higher temperatures raised serious safety, reliability, and maintenance issues, limiting their widespread application [16,18]. Overheating and thermal management are major hurdles to be addressed in high-temperature NaSBs (HT-NaSBs) operated above 300 °C with molten electrodes. Subsequent research strategies to explore the chemistry of sodium and sulfur reliably and sustainably led to the development of RT-NaSBs [19]. A typical RT-NaS cell consists of a metallic sodium anode, a sulfur-carbon composite cathode, and an organic liquid electrolyte as a separator, as illustrated in Figure 2a [20]. In contrast to the HT-Na-S batteries, where Na_2S_3 is the final discharge product on account of thermodynamic limitations, Na_2S forms the final discharge product in RT-NaSBs as its formation is thermodynamically feasible at room temperature, leading to a higher theoretical capacity [17]. Furthermore, in RT-NaSBs, a series of intermediate reactions occur during the complete transformation of S_8 to Na_2S [18]. More importantly, the RT working environment significantly reduces the concerns of burning or explosions caused by the highly reactive molten Na and S. Furthermore, the maintenance cost could be reduced mainly by operating at room temperature, favoring extensive energy storage applications [17,21].

A complex transformation of longer-chain polysulfides to short-chain polysulfides occurs in RT-NaSBs during the discharge process via a dissolution/precipitation reaction giving rise to severe challenges (which will be discussed later in detail) to achieving reliable cycle performances and efficiency [22]. During the discharge process (sodiation), the higher order polysulfides (Na_2S_n, $4 \leq n \leq 8$) formed at the cathode side, become dissolved in the liquid electrolyte, and migrate to the anode side. These dissolved polysulfide species are reduced at the anode side finally as lower order polysulfides (Na_2S_n, $1 \leq n \leq 4$), which are insoluble [22]. The typical RT-NaSBs display two plateaus (see Figure 2b) located at 2.2 V and 1.65 V during discharge and at 1.75 V and 2.4 V during charge. Figure 2c shows the characteristic cyclic voltammetry (CV) profile of the RT-NaSBs. The various NaPS intermediates formed during the electrochemical reaction of sodium and sulfur are listed in Figure 2b, along with the corresponding theoretical capacities. Interestingly, the redox process in RT-NaSBs consists of complicated intermediate stages where the soluble liquid phase polysulfides and the insoluble solid phase polysulfides coexist [22]. Moreover, the final stage is a kinetically retarded phase where non-conducting solid-phase NaPSs are formed. Henceforth it is challenging to practically achieve the high theoretical energy density of RT-Na-SBs of 1274 Wh kg^{-1} (based on the mass of both sodium and sulfur) [17,23].
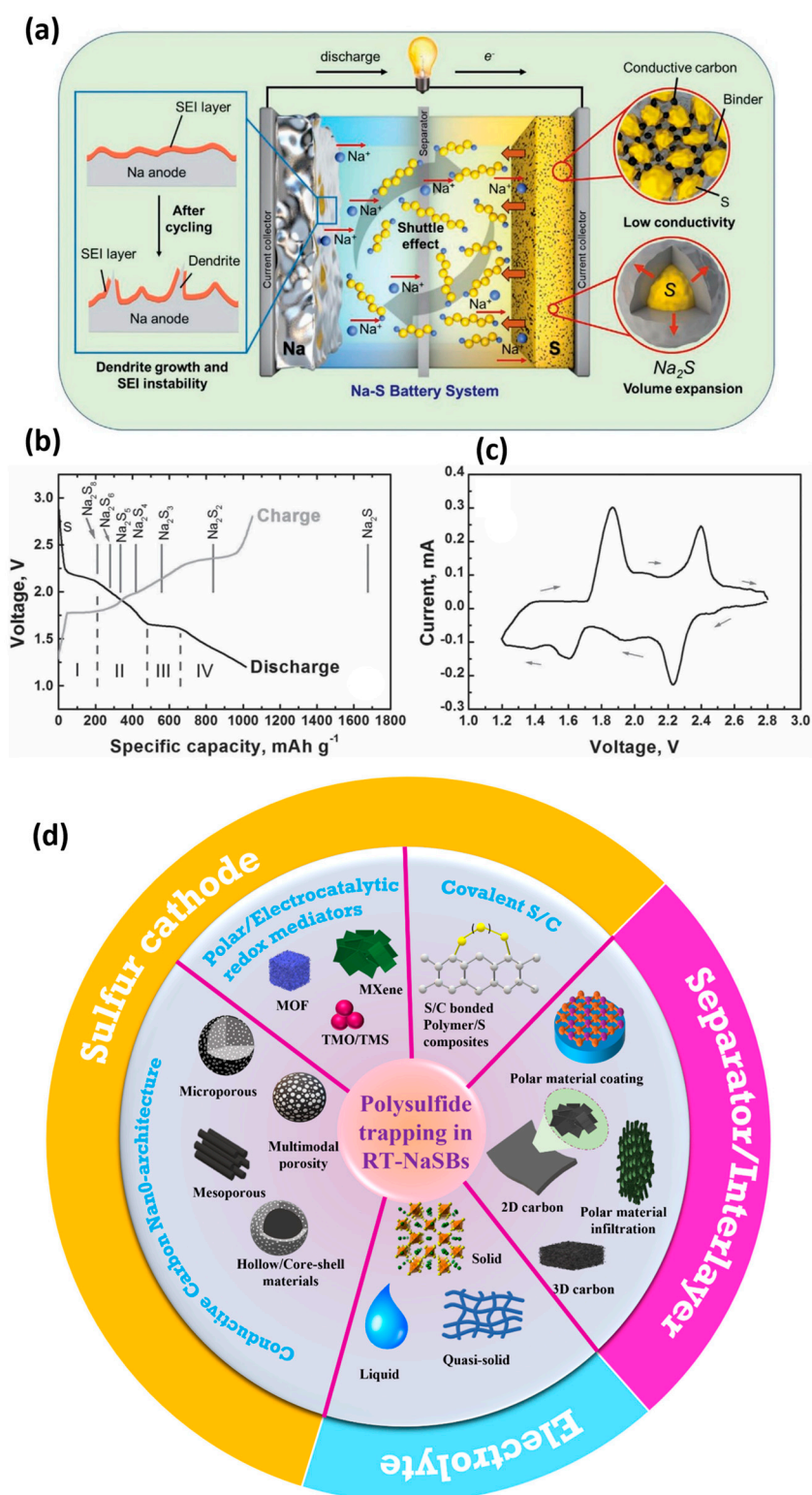
Figure 2. (**a**) Schematic illustration of RT-NaSBs. Reproduced with permission [21] Copyright 2021, Wiley. (**b**) Typical voltage and (**c**) CV profile of RT-NaSBs. Reproduced with permission [24]. Copyright 2015, Wiley. (**d**) Schematic illustration of the NaPS adsorption strategies employed in RT-NaSBs.

3. Challenges in RT-NaSBs

Even though RT-NaSBs have been reported since 2006, there are many critical challenges to be addressed to realize the projected applications of this system [19]. The cell chemistry of RT Na-SBs is much more complex and raises many more hurdles for practical applications, considering the reversibility of the reaction, electrochemical sulfur utilization, and protection of metallic Na anode.

3.1. Sulfur Cathode

The nonconductive nature of elemental sulfur (5×10^{-28} S m^{-1}) has been identified as one of the major issues generally compensated by the utilization of conductive carbon matrices to encapsulate the sulfur species [25]. However, this strategy leads to lower utilization of the active material and thereby reduces the cycle life and volumetric capacity. The lower-order NaPS species (Na_2S, Na_2S_2), which are the final discharge products of the RT-Na-S system, are also nonconducting in nature, raising further challenges to capacity retention and long-term cyclability [26]. Additionally, the huge volume expansion in the RT-NaSBs (171% upon full sodiation) and the sluggish transformation kinetics of the NaPS severely affect the reversibility of redox reactions [22].

3.2. Electrolytes

Analogous to the LSBs, the major technological challenge faced by the RT-NaSBs is the polysulfide shuttle mechanism which leads to low efficiency and rapid capacity fade upon cycling [27,28]. The NaPS species generated during the discharge process dissolve in the liquid electrolyte and migrate to the anode side, initiating uncontrolled parasitic reactions. Furthermore, the passivation of the anode surface due to the deposition of NaPS species can lead to an internal short circuit of the cell. Overall, the NaPS shuttle in RT-NaSBs lead to severe capacity decay and self-discharge phenomenon, ultimately resulting in low active material utilization [29].

3.3. Metallic Na Anode

The major challenges to be addressed in the anode involve the continuous consumption and loss of Na metal due to the make–break cycle of a solid electrolyte interphase (SEI) layer during the charge/discharge process [30]. The nonhomogeneous plating/stripping of Na$^+$ can also result in eventual dendritic growth, shorting the cell internally [31].

4. Electrode and Interfacial Engineering for Polysulfide Shuttle Inhibition and Polysulfide Trapping

NaPS generation and dissolution are critical issues that degenerate the cell efficiency of RT-NaSBs. The rational implementation of innovative polysulfide adsorption and trapping mechanisms employing the concept of the electrode and interfacial engineering can considerably improve cell performances. Electrode engineering is a practical approach that can be employed in RT-NaSBs, wherein the electrode components such as the S cathode, separators, and electrolytes can be extensively modified strategically to improve the electrochemical performances of the resultant cells. An additional interlayer configuration can also be employed in RT-NaSBs to block the PS species similar to that in LSBs. Such approaches encompassing the concepts of electrode/electrolyte interfacial engineering can be significant in mitigating PS shuttling. The highly reactive Na anode is also a major component that limits the performance of RT-NaSBs, due to the formation of unstable interfaces that propagates dendritic growth. Henceforth, it is essential to employ the concepts of the electrode and interfacial engineering in RT-NaSBs, to improve the reversibility and cyclability by limiting the PS dissolution and dendrite formation.

As NaPS generation and dissolution are critical issues that degenerate the cell efficiency of RT-NaSBs, the rational implementation of innovative polysulfide adsorption and trapping mechanisms is critical to improving cell performance. The polysulfide adsorption and trapping strategies employed in RT-NaSBs can be generally categorized into (a) physi-

cal and (b) chemical methods based on the interaction with the PS species. A plethora of research work has been carried out in both these directions showcasing near-successful mitigation of the shuttle phenomenon. The schematic illustration in Figure 2d shows the rational employment of these strategies in S cathodes, separators/interlayers, and (c) electrolytes to achieve effective polysulfide trapping and, henceforth, excellent electrochemical performances in RT-NaSBs.

4.1. Engineered Sulfur Cathodes

4.1.1. Cathodes with Conductive Carbon Matrices as S Hosts

Nanoengineered carbon matrices with multi-dimensional porosity: Based on the prior knowledge of Li/S technology, various conductive carbon/carbonaceous materials, including carbon nanotubes (CNTs) [32], graphene [33], carbon nanofiber cloths [34], ordered mesoporous carbons (OMC) [21], metal-organic framework (MOF)-derived carbon [35,36], and waste biomass-derived carbon [37] have been investigated in the RT-NaSBs. Apart from boosting electronic conductivity, nanoengineered carbon materials can physically block the generation, dissolution, and migration of PS species via efficient nanostructural confinement of S. The key to this strategy is the creation of diffusion barriers via one-dimensional (1D), two-dimensional (2D), and three-dimensional (3D) structures with controlled pore sizes (micro, meso, macro) and pore structures [38]. The 1D carbon nanostructures offer rapid conversion kinetics of S species facilitated by the accelerated transfer of electrons/ions via 1D transport pathways [32,39], while the 2D structures with elevated surface area and tunable porous structures provide abundant active sites for redox reaction [38,40]. Further, the 3D carbon structures can accommodate active materials well within them, improving the S loading. The excellent electrolyte percolation pathways in them facilitate good contact with the S species, though the adsorption and trapping of NaPS species is precisely dependent on the pore sizes and pore structures involved [41,42].

Generally, the weak interaction between nonpolar carbon and polar polysulfides coupled with the larger size of mesopores and macropores result in the dissolution of higher-order polysulfide species into the electrolyte during the discharge (sodiation) process, which initiates the shuttle phenomenon. For instance, Wang et al. reported a dual physical confinement strategy employing interconnected mesoporous carbon hollow nanospheres (iMCHS) as S hosts with high tap density, wherein the inner hollow spaces accommodate high sulfur loadings while the outer carbon nano shells confine the polysulfides [43]. The system followed a reversible reaction mechanism between Na_2S_x (x = 8, 6, and 5) to Na_2S_4 and then to Na_2S during sodiation and from Na_2S_4 to S_8 during the desodiation process, which was confirmed via in situ synchrotron studies. It can be observed that, despite this sophisticated cathode structure and one-step desodiation process, the electrochemical performance was limited, retaining 292 mAh g^{-1} based on sulfur (unless otherwise mentioned, all the capacity, current density, and energy density values reported in this article are based on active sulfur in the electrode) after 200 cycles.

Among the porous carbon materials investigated, microporous carbons offer excellent polysulfide trapping due to the unique cell chemistry of small S molecules (S_n, n $\leq$ 4), limiting the formation of insoluble intermediate NaPS (Na_2S_n, n > 2) within the micropores. The small pore sizes and high specific surface areas, typical of microporous carbons, provide huge volumes for adsorption and S confinement. The spatial confinement of S molecules in such pores (<0.7 nm) initiates an exceptional "quasi-solid state" redox mechanism between sulfur and S^{2-}/S_2^{2-} species, avoiding the generation of long-chain polysulfides and the detrimental shuttle effect. The direct interaction with the confined S molecules and the desolvated solvent molecules (~0.7 nm) on the exterior of the micropores can alleviate the generation of higher-order polysulfides outside the micropores. Exploring this concept, a coaxial cable-like structure with a pore size of ~0.5 nm consisting of a carbon nanotube inside and an S containing microporous carbon sheath outside (S/(CNT@MPC)) was investigated in a carbonate-based electrolyte [32]. The CV and voltage profiles of this system were significantly different from that of typical S/C composites, advocating

a two-stage conversion of S to Na$_2$S (Figure 3a,b) achieved with pore size control. The reduction of molecular S within the micropores was validated via theoretical studies, and the resultant cathode displayed stable cycling for 200 cycles at a 1 C rate with 63% retention. Similarly, a low-cost, sugar-derived microporous carbon template S host (Figure 3c) also reported an exceptional cyclability (1500 cycles), retaining 300 mAh g^{-1} at a 1 C rate, though the S content was limited to 35% [44]. The impact of pore structure on the mitigation of NaPS in RT-NaSBs was also demonstrated recently, employing a facile coffee residue derived activated ultra-microporous coffee carbon (ACC) with a slit pore (2D) structure, as illustrated in Figure 3d, hosting small sulfur molecules (S$_{2-4}$) [37]. An ultra-stable cyclability with almost no capacity fading was achieved for this composite after 2000 cycles at a 1 C rate with an S loading of 40% (Figure 3e). An improved S loading (44%) reported by Zhang et al. employing a hierarchical double carbon-shell porous carbon microsphere (PCM) consisting of micro-sized carbon shells on the outside and consisted of carbon nanobeads with hollow structure inside as the S host [45]. However, the cycle performances were poor and unsatisfactory (290 mA h g^{-1} at 100 mA g^{-1} after 350 cycles), emphasizing the limitations associated with increased S loadings in microporous carbon structures. To summarize, though the S/microporous carbon cathodes displayed overall stability and long-term cyclability, the low S content (<45%) in electrodes is a major drawback. The low S loadings along with the low operating voltage obtained via the quasi-solid-state reaction lower the achievable energy density, inhibiting practical applications. To tackle this issue, hybrid S electrodes designed with both micro/mesopores can increase the S loading capability in electrodes.

Hetero atom-doped carbon matrices: Hetero atom doping is a widely adopted strategy to improve the physiochemical properties of carbon materials [46,47]. It is achieved by modifying the electronic structure of carbonaceous materials and enhancing the conductivity, charge transfer properties, and reaction kinetics [48]. Notably, the introduction of hetero atoms (single metal atom or non-metal atom) in carbonaceous S hosts can induce strong polar interactions with polysulfide species, as opposed to conventionally nonpolar carbon matrices [49–51]. The simple modification with various non-metallic atoms offers good polysulfide adsorption capability without compromising the energy density. Nitrogen (N) is the most commonly employed dopant in carbon materials owing to the high electronegativity of N atoms [52–54]. N-doped nanoporous carbon synthesized by the carbonization of metal–organic framework zeolitic imidazolate framework (ZIF-8) with pyridinic and pyrrolic-N groups reported decent cyclability, retaining 500 mA h g^{-1} at 0.2 C after 250 cycles [36]. Further, the reduction in conductivity upon increasing the N-doping was investigated in detail by Eng et al. [55]. Pyridine *N*-oxide was found to have the most robust binding with discharged species due to polar–polar interactions, followed by pyrrolic and pyridinic N-groups. These polar interactions arise as a result of the presence of lone electron pair on the nitrogen atom in pyridinic N, the polar N–H bond in pyrrolic-N with a high dipole moment, and the lone electron pairs on the oxygen atom in pyridine *N*-oxide, facilitating excellent polysulfide adsorption. The preferential binding of NaPS with these N-groups, obtained at lower carbonization temperatures, was validated via density functional theory calculations, indicating that despite the lower conductivity, N-doping should be prioritized to mitigate the shuttle phenomenon and extend the cycle performances. Excellent reversibility was observed for the composite cathode, retaining 800 mAh g^{-1} after 800 cycles.
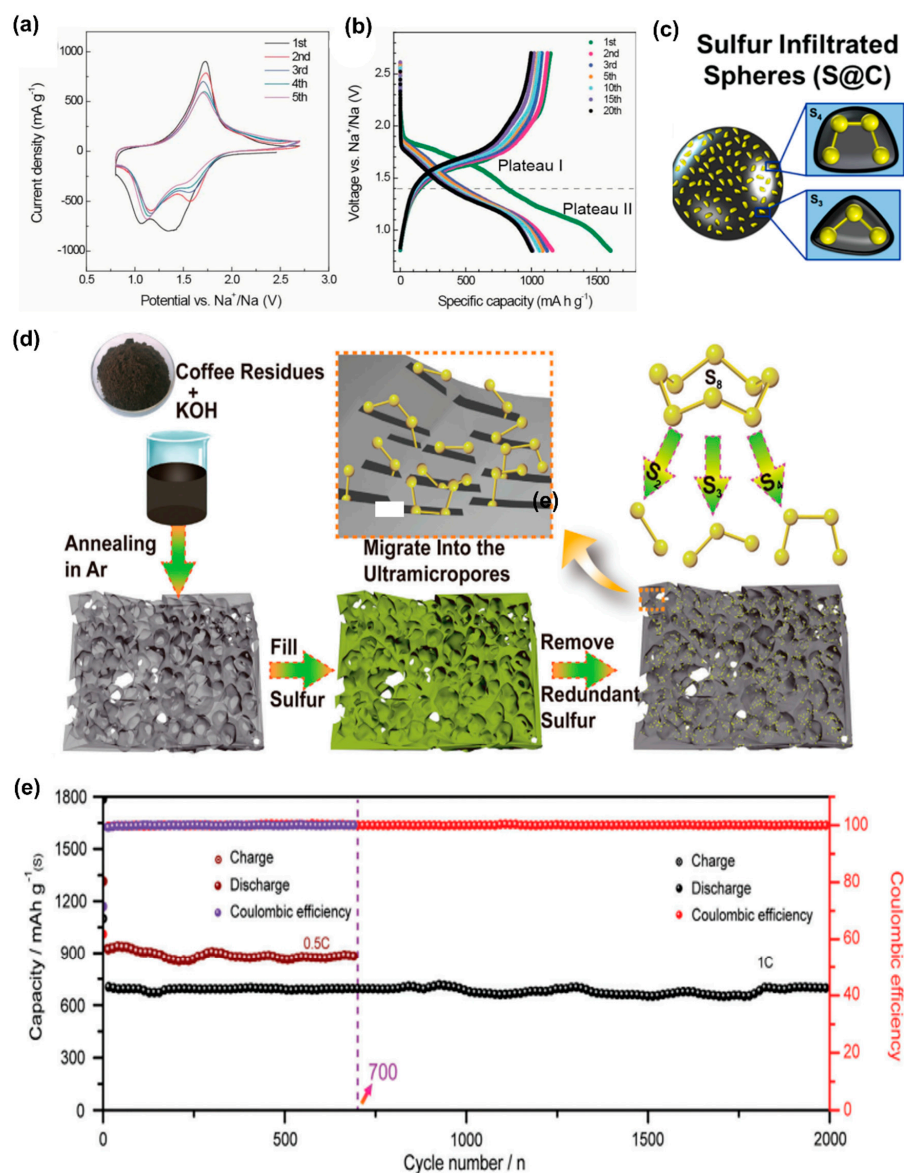
Figure 3. (**a**) CV and (**b**) voltage profiles of RT-NaSBswith sulfur encapsulated microporous carbon sheath electrode. Reproduced with permission [32]. Copyright 2014, Wiley. (**c**) Sucrose infiltrated microporous carbon structure. Reproduced with permission [44]. Copyright 2017, American Chemical Society. (**d**) Schematic illustration of S encapsulated in 2D slit pores of coffee-derived carbon and (**e**) the corresponding cycle performance [37].

Co-doped carbon structures have shown enhanced electron transfer properties resulting in exceptional performances in alkali-ion-based batteries [56,57]. Adopting this strategy, Xia et al. reported an N, O co-doped 1D carbon nanostructure consisting of carbon hollow nanobubbles on porous carbon nanofibers (CHNBs@PCNFs) utilizing a simple electrospinning technique adjusting the heating rates and the metal azide content (Figure 4a) [58]. The strong interactions between the generated NaPS and the N, O atoms enabled excellent confinement of NaPS species within the cathode. The DFT analysis revealed that N/O co-doping enhances the affinity to Na_2S, Na_2S_4, and Na_2S_6 systems compared to single atom doped (N-doped, O-doped) and non-doped carbon. When exposed to NaPSs, the CHNBs@PCNFs with N and O co-doping displayed lower adsorption peak for NaPS in UV–vis spectroscopy studies (Figure 4b), which could be correlated to stronger NaPS adsorption in the sample. Similar observations were reported in another study wherein multichambered carbon nano boxes (MCCBs) synthesized with N, O co-doping (Figure 4c)

confirming the strong chemical affinity of N, O groups to NaPS [59]. A low-capacity (0.045% decay per cycle) over 800 cycles at 5 A g^{-1} was achieved in the work. These studies indicate that introducing co-doping in carbon matrices can be beneficial to achieving stronger adsorption capability towards NaPSs.

Apart from the non-metallic atomic dopants, single metal atom doping has been found to be exceptionally effective for both polysulfide adsorption and catalytic redox mediation. An atomic Co atom incorporated hollow carbon sphere (S@Co$_n$−HC) was introduced as an S host retaining 508 mA h g^{-1} at 100 mA g^{-1} after 600 cycles [60]. The strategy benefits from the utilization of atomically dispersed Co as an efficient electrocatalyst, facilitating fast PS transformation. The reduction of Na$_2$S$_4$ into Na$_2$S by the atomic Co employed within the S host was investigated via a combination of spectroscopic and theoretical studies such as operando Raman spectroscopy, synchrotron X-ray diffraction, and density functional theory (DFT). Followingly, a single Fe atom anchored N-doped mesoporous hollow carbon (NMC) consisting of atomically dispersed dual active sites (Fe–N$_4$) was also investigated [61]. The Fe-N$_4$ sites in the carbon matrix were found to enable advanced chemical adsorption of polysulfide species, boost the electron (e^-) transfer, and facilitate excellent Na diffusion to the Na-poor regions, enabling the rapid conversion of intermediate NaPS species to Na$_2$S, in contrast to the conventional N-doped carbon cathodes where distinct separation between Na-rich and Na-poor regions prevails. With this feature, the reaction kinetics and the reversible capacity of RT-NaSBs with Fe-N$_4$ sites were enhanced considerably, resulting in long-term cycle performances (540 mAh g^{-1} after 500 cycles at 100 mA g^{-1}).
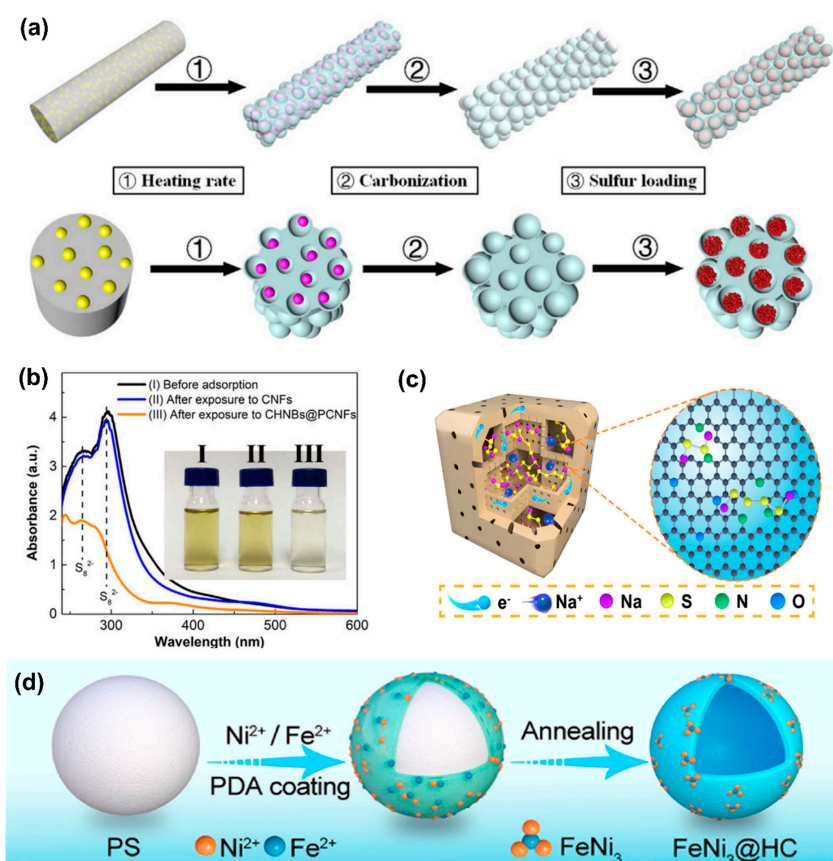

Figure 4. (**a**) Carbon hollow nanobubbles on porous carbon fibers as S hosts, and (**b**) the demonstration of PS adsorption capability via UV spectroscopy. Reproduced with permission [58]. Copyright 2018, Elsevier. (**c**) Multichambered carbon nano boxes synthesized with N, O co-doping. Reproduced with permission [59]. Copyright 2021, American Chemical Society. (**d**) FeNi$_3$@hollow porous carbon spheres as S hosts. Reproduced with permission [62]. Copyright 2021 American Chemical Society.

Polar and electrocatalytic redox mediator encapsulations: Recently, the incorporation of polar materials into the carbonaceous S hosts to compensate for the weak affinity of non-polar conductive carbons to NaPS species has been explored widely to inhibit NaPS dissolution and the shuttle effect. The strong affinity of polar materials to NaPS species via polar-polar interactions results in effective adsorption of NaPS via chemical coupling. The polar material-incorporated carbonaceous S hosts benefit from both physical (nanostructural confinement) and chemical (polar interaction) PS adsorption, improving the electrochemical performance of RT-NaSBs. Following the established concepts of PS mitigation in LSBs, many polar materials, including metallic nanoclusters, metal oxides, metal chalcogenides, metal carbides, and MOFs, have been investigated in RT-NaSBs so far. The electrocatalytic ability of transition metal and metal oxide nanoparticles to boost redox kinetics has become a hot topic of interest. First among such initiatives in RT-NaSBs involve a nano-copper-assisted S immobilization method demonstrated by Zheng et al. confining S in a high-surface-area mesoporous carbon host with 50% S loading [63]. The inclusion of 10% nano Cu in the composite facilitated the immobilization of active S species within the cathode structure via the formation of CuPS on account of the strong interactions between Cu and S.

Among the various transition metal catalysts reported for RT-NaSBs, nickel (Ni) has been proven to efficiently adsorb the NaPSs and accelerate the electrochemical kinetics of NaPSs transformation [64]. The introduction of bimetallic alloys is another strategy to enhance carbonaceous S hosts' electronic properties further. Wang et al. reported a $FeNi_3$@hollow porous C/S host (Figure 4d) displaying an excellent electrocatalytic effect [62]. The NaPS precipitation capacity of $FeNi_3$@HC was found to be much higher than the pristine hollow porous C/S composite and the one containing only nickel demonstrating the firm anchoring of long-chain NaPSs and their rapid conversion to short-chain NaPSs. A 3D hierarchical S cathode (40% S loading) consisting of an in situ grown vanadium dioxide (VO_2) nanoflower catalyst on rGO reported the accelerated conversion of long-chain NaPSs to Na_2S_2/Na_2S via the catalytic effect of VO_2 (Figure 5a) [65]. The rGO/VO_2/S composite retained 156.1 mA h g^{-1} after 1000 cycles at 2 C, exhibiting 0.07% capacity decay per cycle. Similarly, Kumar et al. demonstrated a free-standing manganese dioxide (MnO_2) decorated carbon cloth (CC@MnO_2) as a "sulfiphilic matrix" and polysulfide reservoir, employing an unconventional sodium polysulfide (Na_2S_6) catholyte as the active material in contrast to the melt-diffused S species [66]. The capacity retention of 67% after 500 cycles was achieved for this binder-free electrode maintaining a high energy density of 728 W h kg^{-1}. The XPS investigations revealed mechanistic insights into the enhanced catalytic adsorption capability of MnO_2 nanoneedles. Accordingly, in situ formation of polythionate complexes via the electrostatic interaction between the anchored NaPSs on the MnO_2 surface, and the following surface reaction of NaPSs with Mn^{2+}, aid to anchor the high-order NaPSs (Na_2S_n, $4 \leq n \leq 8$), further promoting their electrocatalytic conversion to insoluble short-chain NaPSs.

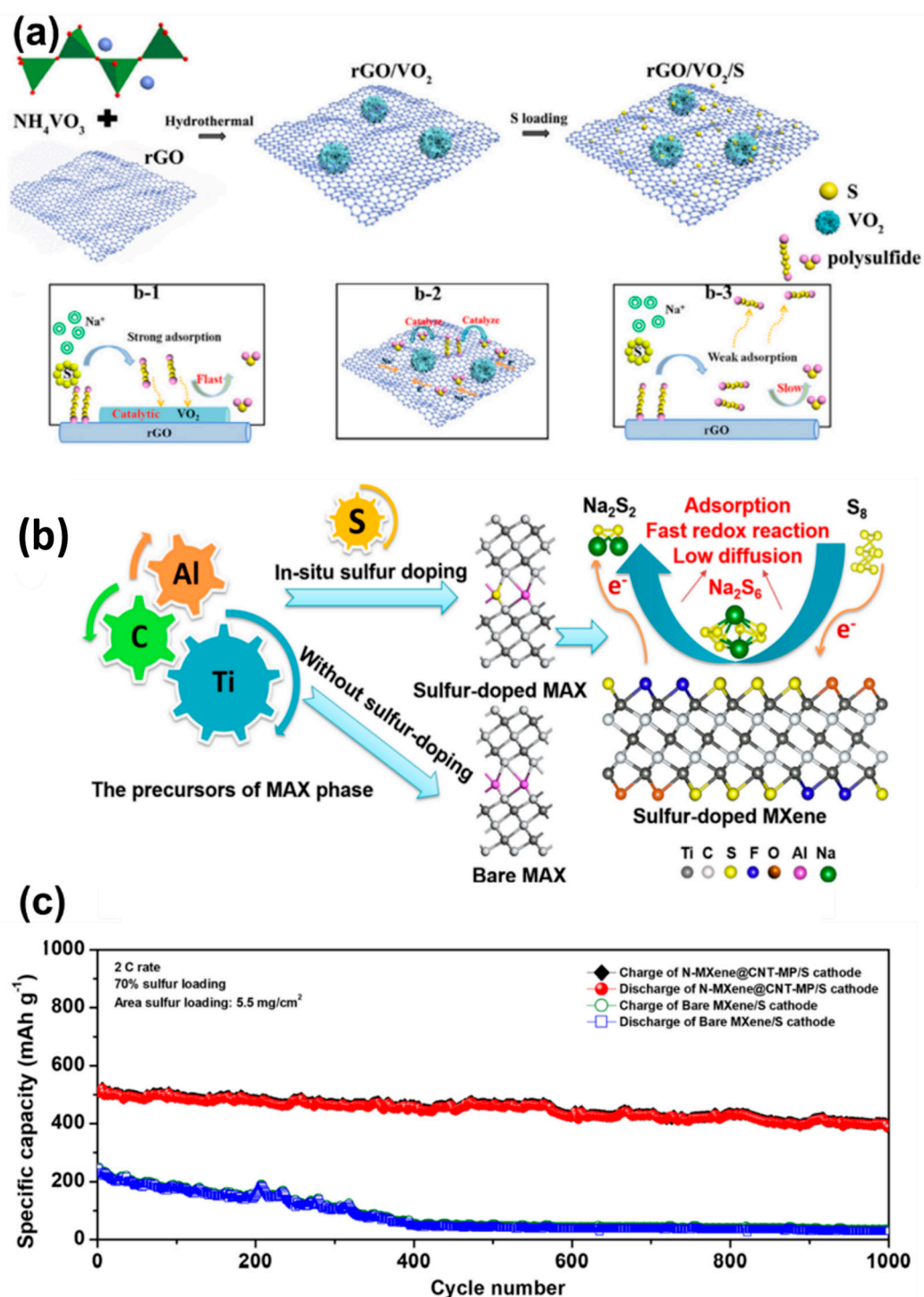**Figure 5.** (**a**) VO$_2$-embedded rGO. Reproduced with permission [65]. Copyright 2019, Elsevier. (**b**) Sulfur-doped MXene [67]. Copyright 2019, American Chemical Society. (**c**) Cycle performances of N-doped Ti$_3$C$_2$T$_x$ MXene microspheres. Reproduced with permission [68]. Copyright 2021, American Chemical Society.

MOF-derived carbon materials find immense applications in various fields due to their exceptionally high surface area, uniform pore structures, atomic-level structural uniformity, and tunable porosity [69–71]. The increased surface area of MOF-derived carbon materials facilitates enhanced S loadings and can accommodate the volume changes during cycling [72,73]. Additionally, in situ doping with heteroatoms can be achieved by the carbonization of heteroatom-containing MOFs, which improves the electrical conductiv-

ity and adsorption ability of the S host [74]. Synthesis of sophisticated hybrid materials involving transition metal or transition metal chalcogenide (sulfide and selenide) embedded MOF-derived carbon materials benefit from the good catalytic absorptivity of chalcogenide species and the physical confinement of S within the MOF-derived microporous carbons [75–77]. For instance, flexible and freestanding porous nitrogen-doped carbon nanofiber (PCNF) encapsulating Co nanoparticles (Co@PCNFs, Co = 15.7%) were reported recently by Yang et al., with a high S loading of 2.1 ± 0.2 mg cm^{-2}, enabled the activation of S species via electron engineering [78]. This hybrid composite was synthesized by carbonizing an electrospun Zn, Co−ZIF/PAN nanofiber mat and could accommodate almost 60% S content. UV–vis studies for NaPS adsorption along with density functional theory calculations, demonstrated the successful boosting of transformation kinetics of higher-order polysulfides to Na_2S via the embedded metallic Co nanoparticles. Good cyclability was achieved for this hybrid cathode, retaining 398 mA h g^{-1} at 0.5 C over 600 cycles, which accounts for the best electrochemical performance in freestanding electrodes for RT-NaSBs so far. Similarly, a mesoporous cobalt sulfide/nitrogen-doped carbon (CoS_2/NC) was synthesized as an S host by the sulfurization of a polydopamine-coated Co−MOF [79]. The catalytic properties of CoS_2 were verified by DFT analysis. A correlation between the pore size and the presence of short-chain NaPS was elucidated by tuning the pore size in the composite via the introduction of Zn^{2+} and the selective removal of ZnS. The degree of the catalytic effect depended on the proximity of CoS_2 to the sulfur. Followingly, a dual metal sulfide encapsulated multisulfiphilic S cathode was fabricated by Hanwen et al. consisting of porous core–shell carbon structure and multisulfiphilic sites of ZnS and CoS_2, which can promote the electrocatalysis of S species by suppressing the dissolution of long-chain polysulfides and improving the transformation kinetics of short-chain polysulfides [80]. Long-term cycle performances of this dual metal sulfide incorporated S cathode retained 250 mAh g^{-1} at 1.0 A g^{-1} over 2000 cycles. Yolk-shell FeS_2/C hollow nanocubes embedded in hollow carbon fibers as cathode and FeS_2@C/CNT along with a CNT hybrid film as the modifying layer on the separator were demonstrated recently for flexible RT-NaSBs [81]. Benefitting from this unique design strategy with a dual defense system, long-term cycle performances were achieved with a maximum S loading of 7.6 mg cm^{-2}, retaining an ultralow capacity decay rate (0.024%) after 1000 cycles at 2 C.

MXenes are two-dimensional (2D) inorganic compounds, e.g., transition metal carbides and nitrides, which are a few atoms thick, with the general formula, $M_{n+1}X_nT_x$, where M is a transition metal such as Ti, Cr, V, Mo, Nb, etc., X is either carbon or nitrogen, and T_x denotes the terminal functional group (F, O, and OH) [82]. The first report of MXenes dates to 2011, and they are currently being investigated for diverse applications in energy storage and catalysis [82–84]. This class of 2D materials benefits from active functional surfaces, high electronic conductivity, and chemical durability that favor their applications in RT-NaSBs. The synthesis of MXenes typically involves the selective etching of the A element in the corresponding $M_{n+1}AX_n$ phases, where A is an element from IIIA or IVA (Al, Ga, Si, S) sandwiched between the M and X layers. In such an attempt, Bao et al. reported a 3D wrinkled MXene nanosheet (S–$Ti_3C_2T_x$) prepared via doping MXenes with S atoms [85]. S-atom-doped MXene enhances the redox activity of RT-NaSBs and enables the controlled diffusion of NaPS species into the electrolyte, resulting in high-rate capability. DFT investigations revealed the preferential binding of NaPS species to the surface of S–$Ti_3C_2T_x$ composite which correlated well with the long-term cyclability of the cell, denoting NaPS shuttle-free operation. Raman studies of the S–$Ti_3C_2T_x$ electrode before and after cycling further confirmed the generation of NaPS species during discharge and its adsorption by the S–$Ti_3C_2T_x$ nanosheets. Self-assembled, porous nitrogen-doped $Ti_3C_2T_x$ MXene microspheres reported by a modified spray drying and annealing method could achieve a high sulfur loading of 5.5 mg cm^{-2} [67]. The N-doped cathode structure exhibited strong affinity to NaPSs via Na–N and Ti–S interactions, resulting in highly efficient binding toward NaPSs. Exceptionally stable high-rate cycling performance was achieved for the S–$Ti_3C_2T_x$ electrode, retaining 450.1 mAh g^{-1} at 2 C after 1000 cycles (Figure 5b).

4.1.2. Covalently Bonded S/C Cathodes and S Copolymers

Carbon materials containing active sulfur species covalently bound to polymeric carbon backbone have been extensively investigated recently [68,86–88]. The covalently bound S–C composites display excellent reversibility and shuttle-free operation on account of the direct solid-to-solid conversion reaction during redox reaction, completely unlike that of conventional S/C composites. In general, the covalent S–C composites are prepared by in situ synthesis methods employing closed systems with an inert atmosphere as ex situ S–C bonding strategies may result in incomplete and non-homogeneous covalent binding of sulfur to the C backbone and lead to the undesirable formation of elemental S on the composite surface, adversely affecting the electrochemical performances. Further, the covalently bound S/C composites exhibit good compatibility with carbonate-based electrolytes, which are utilized in commercial batteries, unlike the traditional S cathodes, which employ ether-based electrolytes [89].

Among all the covalently bound S/C composites, sulfurized polyacrylonitrile (SPAN) is the most interesting and extensively investigated S/C composite. SPAN is prepared by the pyrolysis of S and PAN, during which the dehydrogenation and cyclization of PAN occur, and the S atoms are covalently linked to the carbon atom in the polypyridine ring backbone [90]. The SPAN cathode exhibits good long cycle life and rate performances compared to conventional S/C cathodes and utilizes a carbonate-based electrolyte [91,92]. For example, an electrospun 1D fibrous SPAN cathode reported by Hwang et al. displayed robust cycle performances such that 70% of the capacity in the fifth cycle was retained after 500 cycles, ultimately alleviating the PS shuttle effect [93]. However, the S content was compromised (<35%) and was not appreciable for practical applications. A singular flexible SPAN cathode prepared by Kim et al. also reported stable cycle performances [94]. Recently, doping of SPAN cathodes with trace amounts of tellurium [95], iodine [96], and selenium [97] as eutectic accelerators have been explored to improve the reaction kinetics and sulfur utilization. Figure 5c shows the schematic illustration of rapid ion/electron transfer achieved with a tellurium-doped SPAN cathode. In a recent report, Hun et al. reported the insertion of the maximum number of Na atoms into the SPAN cathode by extending the discharge to 0.01 V, as opposed to previous studies [92]. The SPAN electrode exhibited a reversible capacity of 1502 mAh g^{-1} (~90% of the theoretical value) and retained 1405 mAh g^{-1} at 0.16 C rate even after 100 cycles. Despite the exceptional cyclability and reversibility observed with such modifications, improving the S content in the SPAN composites beyond 50% remains a major challenge. A new S copolymer cathode reported by Ghosh et al. with an S-embedded cardanol benzoxazine polymer and reduced graphene oxide could achieve an exceptionally high S loading of 90% [98]. The cathode with a unique structure (Figure 5d) was prepared by thermal ring-opening polymerization of benzoxazine in the presence of elemental sulfur and mixed with rGO. Interestingly, the ICP analysis of the electrolyte after the cycling process revealed restricted dissolution of NaPS in this novel composite compared to a conventional S/C cathode, benefiting the chemical binding of S species in the cathode. In another work, organosulfur (e.g., 4-aminophenyl trisulfide ($H_2N–C_6H_5–SSS–C_6H_5–NH_2$)) covalently tethered to the surface of electrically conductive CNT networks was reported by Milan et al., as positive electrodes in an aqueous electrolyte demonstrating reversible surface redox kinetics [99]. Interestingly, unlike traditional RT-NaSBs, the voltage profiles resembled that of a supercapacitor enabling long-term cyclability and high-power density.

Many novel strategies have been put forward to prepare covalently bound S/C cathodes; however, engineering the S content in these unique composites to suit commercial applications is a major hurdle that needs detailed investigation via advanced characterizations. S/C composites generally display a trade-off between conductivity and S contents, as higher annealing temperatures can result in lower S contents. The novel covalent S/C composite prepared by exploiting the strong interaction between carbon disulfide (CS_2) and red phosphorus by a solvothermal method is a classic example [100].

Another novel covalent S-C composite, a thioether bond functionalized carbon (SC) prepared by the carbonization of a crosslinked polymer utilizing thiophene monomer and dimethoxymethane as the crosslinking agent, was reported by Chen et al. [101]. Insoluble NaPS species (Na_2S_2 and Na_2S), which could be hosted within the defects of the pristine cathode, were generated by the cleavage of the thioether bond structure (C–S–C) in a low voltage range of 0.01–0.50 V vs. Na/Na^+ in this system. Excellent reversibility and long-term cyclability were achieved for this cathode material at a high current density of 1 A g^{-1}, exhibiting 330 mA h g^{-1} after 800 cycles with only an undesirably limited S content of 21%. Similarly, the synthesis of a covalent S-based carbonaceous material put forward by Fan et al. utilizing benzo [1,2-b:4,5-b'] dithiophene-4,8-dione also displayed a strikingly minimal capacity decay rate of 0.053% per cycle over 900 cycles, retaining almost 100% CE with only an incredibly low S content (18%) [102].

4.1.3. Dissolved Polysulfide as Cathodes

Advanced hybrid electrolyte configurations incorporating both cathode and electrolyte (catholyte) into a single entity have been thoroughly explored by taking advantage of the dissolved nature of the polysulfides. Such catholyte-incorporated cells can mitigate the whole range of the transformation process of S_8 to higher-order polysulfides during discharge. A multiwalled carbon nanotube cathode with catholyte reported by Yu et al. investigated the lower voltage plateau of RT-NaSBs, avoiding interference from higher-order polysulfides [103]. By preventing this transition that substantially contributes to capacity fade in RT-NaSBs, a stable output capacity for the sulfur/long-chain NaPS redox couple was demonstrated, with a restricted voltage window of 2.8 to 1.8 V. RT-NaSBs with liquid phase NaPS catholyte enclosed in free-standing carbonaceous substrates additionally benefit from the electrode's binder-free nature, which boosts the energy density. An rGO-CNT-CMC substrate prepared by a condensation procedure resulted in a highly cross-linked host, which can mitigate the volume shrinkage due to its sponge-like structure and enable strong NaPS adsorption capability on account of the oxygen functional groups on rGO and CMC surfaces [104]. This quasi-liquid Na/PS battery employing Na_2S_6 catholyte maintained a high sulfur loading (1.9 mg/cm^2) and low electrolyte/sulfur (E/S) ratio (4.05 mL g^{-1}) at room temperature, with a capacity retention of 66.67% after 200 cycles at 0.2 C rate. Additionally, the ultra-low self-discharge of 0.04% per h achieved for this system at open-circuit voltage indicates excellent mitigation of PS shuttle, unlike that in conventional RT-NaSBs.

Free radical catalysis-induced enhancement in reaction kinetics and capacity of NaPS batteries investigated in detail by Kumar et al. utilized a Na_2S_6 catholyte infiltrated activated carbon cloth (ACC) cathode, which displayed remarkably stable cycle performance with a capacity retention of 0.03% per cycle [105]. For the first time, the generation of relatively stable polysulfide radical monoanions ($S3^{\bullet-}$) by the homolytic bond cleavage of polysulfide dianions and the formation of C–S bonds on the surface of the ACC that aids in anchoring the $–S3^-Na^+$ species was validated, facilitating rapid transfer to end products upon discharge. Catalytic adsorption and mitigation of PS species in Na/PS batteries were further explored by incorporating catalytic redox mediators in NaPS hosts similar to the PS mitigation strategies discussed in cathodes as shown in Figure 6a [66]. For example, a manganese dioxide-decorated carbon cloth ($CC@MnO_2$) and a modified $CC@MnO_2$ NaPS host with sodium–alginate nanofibers ($CC@MnO_2@Na–alg$) exhibit the benefits of catalytic redox mediation and PS adsorption [106]. The subzero-temperature (−10 °C) cycling of NaPS cells with an S host consisting of an indium tin oxide (ITO) nanoparticle-decorated activated carbon cloth ($ITO@ACC–Na_2S_6$) was also reported by the same group, showing long-term cycle performances [107]. The remarkable cycle performances (445 mAh g^{-1}) after 1000 cycles at 0.5 C, 20 °C, and 310 mAh g^{-1} after 100 cycles at 0.1 C and −10 °C were achieved for this hybrid system with a high active material loading of 6.8 mg cm^{-2} and is the first report on RT-NaSBs operating at low temperature.
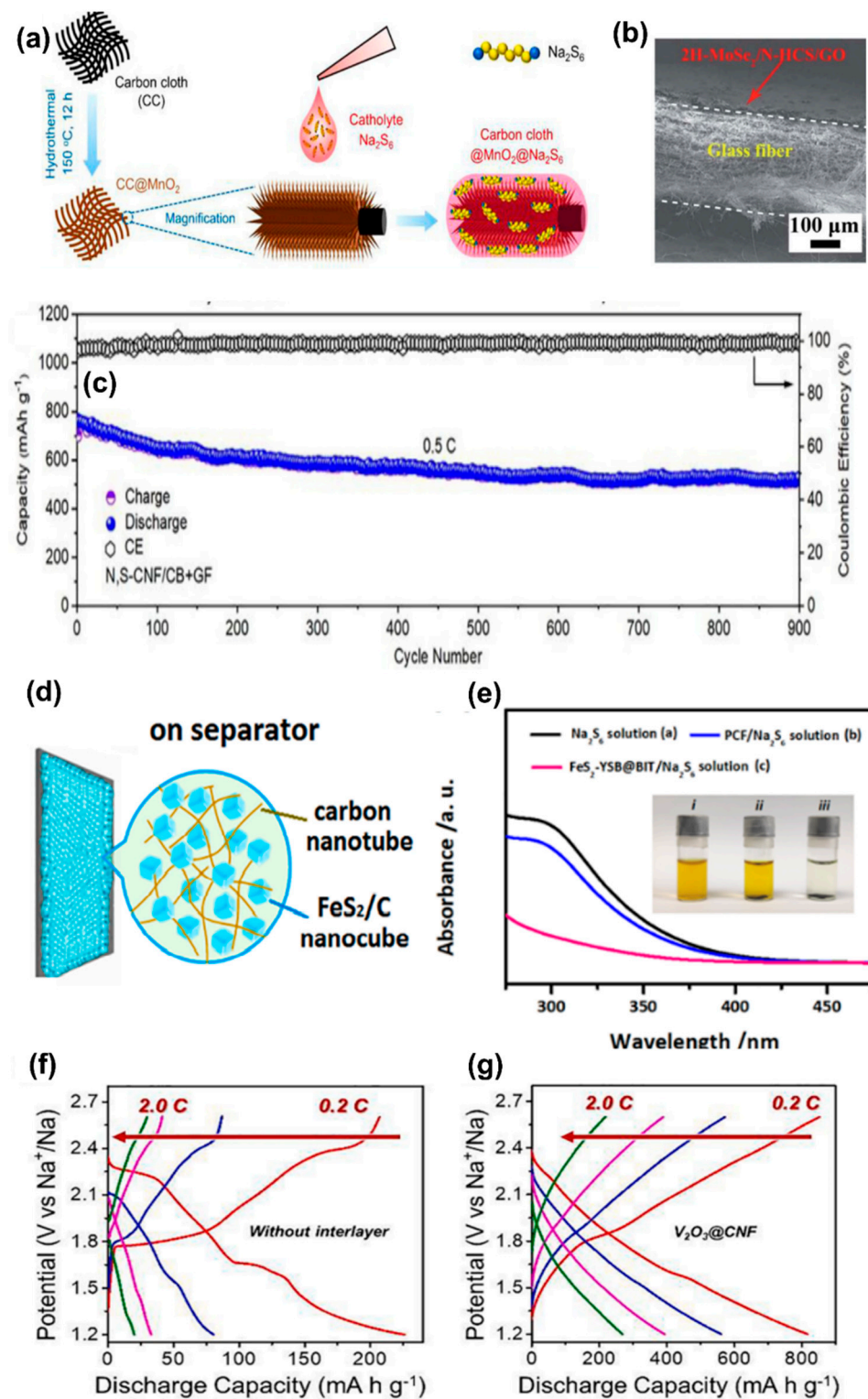
Figure 6. (**a**) CC@MnO$_2$@Na$_2$S$_6$ cathode. Reproduced with permission [66]. Copyright 2019, Elsevier. (**b**) FE-SEM image of MoSe$_2$/N-HCS/GO-coated glass fiber (GF) separators. Reproduced with permission [53]. Copyright 2021, Royal Society of Chemistry. (**c**) Cycle performance RT-Na/S battery with an N, S-CNF/CB+GF separator. Reproduced with permission [108]. Copyright 2022, Elsevier. (**d**) Scheme of FeS$_2$/C nanocube/CNT-coated GF separators and (**e**) demonstration of NaPS adsorption capability. Reproduced with permission [81]. Copyright 2021, Elsevier. Voltage profiles of RT-NaSBs (**f**) without interlayer and (**g**) with V$_2$O$_3$@CNF interlayer. Reproduced with permission [109]. Copyright 2021, Elsevier.

4.2. Modified Separators and Functional Interlayers

4.2.1. Modified Separators

Porous separators with functional modifications, such as coating with polar materials and cation-selective copolymers, have been employed in RT-NaSBs to address the polysulfide shuttle phenomenon. In an earlier report, Bauer et al. put forward the use of a cation-selective sodiated Nafion coating on a porous polypropylene backbone via a drop coating procedure with the aim of not only suppressing the polysulfide shuttle mechanism, but also protecting the sodium metal anode [28]. The cation selectivity of the Nafion membrane allowed the migration of Na^+ cations while repelling the polysulfide anions on account of the negatively charged sulfonic groups in them. The sodiation of the Nafion membrane effectively improved the Na-ion conductivity, thereby improving capacity retention by almost 75% compared to the typical polypropylene separator. Further modifications of a pre-sodiated Nafion membrane with an AC-CNF coating that acts as an upper current collector also reduced the polysulfide diffusion and tremendously improved the sulfur utilization in the Na_2S cathode [103,110]. Other groups have also demonstrated effective NaPS adsorption strategies by directly coating separators with NaPS trapping materials such as Al_2O_3, $MoSe_2$, chelates, and heteroatom-doped carbon materials. For example, a study detailing the incorporation of an Al_2O_3–Nafion membrane printed on GF separator via serigraphy takes advantage of both the ion selectivity of the Nafion membrane and the PS adsorption capability of Al_2O_3 [111]. The membrane thus facilitates the repulsion of the negatively charged NaPS anions (S_n^{-2}) while enabling the Na^+ ion transport. PS adsorption capability of Al_2O_3, and though the ability of the Al_2O_3–Nafion membrane to protect the sodium electrode surface from polysulfide poisoning was clearly established via detailed XPS studies, the study failed to demonstrate good capacity retention and cycle performances.

Improving the cycle life of RT-NaSBs without compromising the S content in the cathode is critical for practical applications. Most of the research works on RT-NaSBs that have demonstrated good cycle life have blatantly compromised the active S content in the cathode. Recently, a few research works have investigated high loading S cathodes for RT-NaSBs, exploring the potential for commercialization. A high S content cathode with a functional separator consisting of $2H$-$MoSe_2$/N-doped hollow carbon spheres/graphene-oxide ($2H$-$MoSe_2$/N-HCS/GO) coated directly onto a GF separator by filtration method demonstrated good cyclability at both low and high current rates (787 mA h g^{-1} at 0.1 C after 100 cycles, 484 mA h g^{-1} at 0.5 C after 500 cycles) [53]. Integrating both physical and chemical NaPS trapping strategies employed in this work resulted in a low-capacity fading rate of 0.077% per cycle, substantiating effective inhibition of NaPS migration to the anode side. Figure 6b shows the FE-SEM image of the $MoSe_2$/N-HCS/GO-coated GF separator. The rapid transformation of Na_2S on the modified separator was evidenced by the FE-SEM images of the anode side of the separator after cycling. The feasibility of this transformation was validated by DFT studies confirming the acceleration of the redox kinetics of the system. Recently, a low-cost alternative to MOF Fe^{3+}/polyacrylamide nanospheres (FPNs) was demonstrated via a facile low-cost separator coating and graphene via vacuum filtration [112]. Interestingly, the RT-NaSBs fabricated with modified separators could achieve good cyclability up to 800 cycles.

Following the trail of PS trapping strategies employed in S cathodes, Dong et al. explored the prospect of NaPS shuttle inhibition by hetero atom-doped carbon for separator coatings. N, S co-doped carbon nanofiber/carbon black (N, S-CNF/CB) composite derived from waste cigarette filters was coated on the GF membrane by filtration method [108]. Long-term cyclability (900 cycles) and a high capacity of 527 mAh g^{-1} were achieved (Figure 6c) with this strategy, maintaining an ultra-low-capacity fading rate of 0.035% per cycle. The rapid conversion of the long-chain NaPSs into the short-chain NaPSs was verified by a first-principle calculation based on DFT. Many researchers have also employed functional separators integrated with modified cathode structures as an additional NaPS defense mechanism. For instance, a hybrid layer comprising of FeS_2/C nanocubes and

conductive CNT coated on GF separators worked in combination with a yolk-shelled hollow FeS_2/C nanocube composite cathode (Figure 6d) as an excellent defense for NaPS [81]. Interestingly, these hybrid Na-S cells exhibited a nominal capacity decay of 0.024% even after 1000 cycles at 2 C rate with a high mass loading of 7.6 mg cm^{-2}. The PS adsorption capability assessed via visual, and UV spectroscopic methods revealed that the NaPS species are completely adsorbed almost within an hour (See Figure 6e).

4.2.2. Interlayers

To tackle the polysulfide shuttle mechanism, some research groups have come up with modifications in the cell structure by incorporating a functional interlayer between the separator and the cathode that can effectively block the NaPS migration to the anode side and simultaneously act as an effective current collector, improving the S utilization in the system. In addition, interlayers can also accommodate the stress and volume expansion encountered during the charge–discharge process in the S electrode, favoring stable cycle performances. Following the trend in LSBs, Yu et al. employed various interlayer *in-house* prepared carbon nanofibers (CNFs), carbon nanotubes (CNTs), and commercially available carbon foams to localize NaPS species [24]. Good active material utilization and improvement in capacity retention were reported for the interlayer incorporated cells. Followingly, the same group reported a carbon nanofoam interlayer between the sulfur cathode and the separator, complemented with an advanced cathode structure [113]. The interlayer accommodated higher-order NaPSs and prevented their migration to the anode. The conductive carbon acted as an effective current collector and improved the sulfur utilization in the system. The flexible carbon foam could also accommodate the stress and volume expansion of the sulfur during the charge–discharge process. This low-cost interlayer configuration improved the capacity retention and cycling stability delivering a stable output energy density of 450 W h kg^{-1} after 50 cycles.

An inorganic filler incorporated polymeric membrane was recently introduced as a blocking interlayer by Saroja et al. [114]. The white graphite (boron nitride) utilized as the inorganic filler effectively trapped the NaPSs due to the presence of boron and nitrogen by chemical adsorption, while the interconnected pores in the white graphite introduced by the polymer blend membrane acted as an ion-selective membrane, facilitating the free movement of Na^+ species. This novel strategy resulted in significant improvement in specific capacity (87.6%) compared to cells without an interlayer and retained excellent capacity retention of 83.1% at the end of 500 cycles. On a similar note, a teflonized carbon substrate was employed as a PS absorbent interlayer by the same group. Though good cycle performances were obtained for the cells, the voltage profile of the system had no significant plateau regions, which was ambiguous [115]. The potential capacity contribution of the teflonized carbon substate was also not investigated in the study. A recent study by Saroha et al. reported a V_2O_3-decorated CNF interlayer demonstrating almost 70% active material utilization at 0.1 C rate [109]. The interlayer configuration was explicitly compared with pristine CNF interlayer and cells with no interlayers in the study, and interestingly, the interlayer incorporated cells did not display the conventional plateau regions (Figure 6f). The voltage profile of the V_2O_3-decorated CNF interlayer is shown in Figure 6g for comparison. Significant changes were detected in V_{2p} and S_{2p} spectra after cycling, which indicated the conversion of higher order NaPS to lower order NaPS and the formation of $S_2O_3^{2-}$ groups, respectively, during the cycling process. However, further investigations of the capacity contribution of V_2O_3 in the system are detrimental to justifying the observed slopy plateau and understanding the complete role of the interlayer configuration in the RT-NaSBs. A catalytic cathode shielding layer (interlayer) consisting of MoO_3/sodium carboxy methyl cellulose slurry coated onto sulfur-incorporated partially exfoliated multiwalled carbon nanotubes (PCNT/S) was reported recently [116]. MoO_3 was utilized as a catalytic redox mediator to enhance the reaction kinetics of the RT-NaSBs and to simultaneously react with NaPS species to form thiosulfate/polythionate complexes, thereby effectively inhibiting their dissolution in the electrolyte. Thus, with

this innovative strategy, capacity enhancement of RT-NaSBs was observed; however, stable cycle performances could not be achieved.

4.3. Novel Electrolytes

The electrolyte acts as a medium of ion transport between the S cathode and the Na anode and forms an integral part of RT-NaSBs. The electrolyte systems are mainly classified into liquid and solid electrolytes. Though liquid electrolytes are ideal for batteries owing to their high ionic conductivities, the issue of NaPS dissolution in liquid electrolytes has prompted RT-NaSB researchers to extensively explore quasi-solid and solid-state electrolytes.

4.3.1. Liquid Electrolytes

Apart from the issue of NaPS dissolution, the main challenge associated with liquid electrolytes in RT-NaSBs is the uneven formation of the solid electrolyte interface (SEI) layer on the Na surface. This leads to an uneven ion flux which further initiates aggressive irreversible reactions of Na metal with electrolyte and prolific Na dendrite growth. The issues mentioned above result in low coulombic efficiency (CE) and can eventually lead to the shorting of the cell. Hence it is crucial to investigate and identify suitable electrolyte components as well as electrolyte additives that can prolong the life of RT-NaSBs.

The tremendous progress in the development of electrolyte systems for RT-NaSBs stems from the thorough investigation and success of ether-based electrolytes, e.g., dimethyl ether (DME) and tetra ethylene glycol dimethyl ether (TEGDME) in LSBs in contrast to the commonly used carbonate-based electrolyte solvents such as ethylene carbonate/dimethyl carbonate (EC/DMC) and ethylene carbonate/propylene carbonate, (EC/PC) in conventional LIBs. Ryu et al. reported initial studies of the charge/discharge mechanism of RT-NaSBs in the liquid electrolyte by using an ether-based TEGDME electrolyte [25]. The discharge plateau had two distinct regions, a sloping region (2.23–1.66 V) and a plateau region at 1.66 V, similar to that of RT-NaSBs reported with polymer electrolytes based on poly (ethylene oxide) (PEO) [117] and poly (vinylidene fluoride) (PVDF) [20,118]. An ether-based electrolyte consisting of sodium trifluoromethanesulfonate ($NaCF_3SO_3$) dissolved in the non-flammable TEGDME solvent displayed a high ionic conductivity ($>10^{-3}$ S cm^{-1}) [119]. The RT-NaSBs assembled using this electrolyte with a hollow carbon sphere/sulfur composite as cathode and a Na–Sn–C anode exhibited a promising reversible capacity of ~550 mAh g^{-1}, establishing a new standard electrolyte for RT-NaSBs.

Sodium salts, such as sodium perchlorate ($NaClO_4$) and sodium hexafluorophosphate ($NaPF_6$), dissolved in ethylene carbonate (EC), propylene carbonate (PC), or dimethyl carbonate (DMC) are generally employed as carbonate-based electrolytes for RT-NaSBs. Interestingly, the first voltage plateau usually observed at 2.3 V in ether electrolytes is absent in the case of carbonate electrolytes, making the discharge profiles significantly different from each other [120]. Another interesting aspect outlined by researchers is the correlation between the type of electrolyte and the form of active S in the electrode. Detailed investigations carried out via ex situ XRD, DSC, and EDS studies at various states of discharge in carbonate electrolyte for a covalently bound sulfurized polyacrylonitrile cathode revealed that the final discharge products formed were Na_2S_3 and Na_2S_2. The compatibility of the microporous S_{2-4} cathode with a carbonate-based electrolyte system was verified via computational studies by Xin et al., affirming the elimination of vigorous NaPS dissolution reactions, unlike conventional ether electrolytes [32]. Apart from their high ionic conductivities carbonate electrolytes are generally appealing for RT-NaSBs, due to their excellent compatibility with sulfur encapsulated as short-chain NaPS (Na_2S_{2-4}) species. However, the substantial compromise on the active S loading in the electrode is a major drawback of this strategy, as discussed in the cathode section.

Employment of suitable electrolyte additives is another effective method to obtain highly stable SEI films and excellent reversible Na deposition even at high current densities, e.g., a tailored ionic liquid-based additive consisting of 10 vol% 1-methyl-3-propylimidazolium-

chlorate tethered to SiO_2 in a blend of EC/PC electrolyte (SiO_2–IL–ClO_4) employed by Wei et al. facilitated the formation of a chemically passivating layer on the Na anode preventing parasitic reactions with the electrolyte [35]. Silica particles introduced to the IL reduced the electric field through the tethered ClO_4^- anions, enabling excellent high-rate cycle performances as shown in Figure 7a (600 mAh g^{-1} at 0.5 C for 100 cycles). Similarly, employing a fluoroethylene carbonate (FEC) additive along with a carbonate-based electrolyte in a recent study resulted in a high reversible capacity of up to 1651 mA h g^{-1} at 0.1 C [121]. Spectroscopic studies of the electrode surface confirmed the formation of a highly stable SEI layer and the reduction of FEC during initial discharge/discharge, leading to the formation of sulfur oxides. The role of indium triiodide, an electrolyte additive and a redox mediator, was explored in another study which demonstrated the rapid kinetic transformation of sodium sulfide while simultaneously building a passivating layer on the anode to mitigate polysulfide corrosion [17]. Indium triiodide additive with a highly concentrated sodium salt in PC and FEC co-solvents dramatically reduced the solubility of NaPS species and enabled the construction of a robust SEI layer on the Na anode leading to stable cycling (Figure 7b). To address the high flammability of carbonate electrolytes in RT-NaSBs, Zhao et al. introduced trimethyl phosphate (TMP) as a flame-retardant (FR) additive into the conventional carbonate electrolyte consisting of $NaClO_4$ in EC/PC [122]. An optimized TMP content of 15 wt.% exhibited non-flammability and facilitated excellent cycling stability for the RT-NaSBs, retaining a reversible capacity of 788 mAh g^{-1} after 80 cycles. Another attempt involving a mixture of TMP, FEC, and trifluoromethanesulfonimide (NaTFSI) resulted in the formation of a NaF-rich SEI layer that further reduced interfacial resistance and suppressed the Na dendritic growth [123].

The utilization of electrolyte additives in ether electrolytes has also proven to be a proficient method to improve the ion transfer properties and reduce NaPS solubility, as in the case of LSBs. Manthiram et al. demonstrated enhancement in capacity by utilizing concentrated sodium salts with $NaNO_3$ additive in TEGDME solvent as an electrolyte, adapting directly from the success of LSBs [110]. This strategy also enabled the construction of a robust SEI layer on the Na anode and achieved a high energy density of 1800 Wh kg^{-1} (first discharge) and 720 Wh kg^{-1} (after 20 cycles). However, the reaction chemistry of the electrolyte combination on the cell's performance was not validated experimentally. Another study employing P_2S_5 as an additive in TEGDME electrolyte proposed by Kohl et al. almost altered the characteristic electrochemical discharge pattern of RT-NaSBs in TEGDME electrolyte [124]. RT-NaS full batteries employing a pre-sodiated hard carbon anode in combination with this tailored novel electrolyte achieved remarkable discharge capacities of up to 980 mAh g^{-1} even after 1000 cycles. A NaI–P_2S_5-based electrolyte additive put forward by Ren et al. enabled excellent capacity retention of 92.9% for 50 cycles at the rate of 0.2 C [125]. The kinetics of Na_2S_2 precipitation was enhanced in the system by forming a soluble Na_2S_2–P_2S_5 complex, while the I^-/I_3 species improved the dissolution of Na_2S_2 via the redox mediation process. Daniele et al. investigated the less explored glyme-based solvent, triethylene glycol dimethyl ether (TREGDME), for RT-NaSBs [126]. The $NaCF_3SO_3$/TREGDME electrolyte displayed low flammability and excellent ionic conductivity (3×10^{-3} S cm^{-1} at 25 °C and 5×10^{-3} S cm^{-1} at 80 °C) and Na-transference number >0.7, validating its potential as a prospective glyme-based electrolyte system for RT-NaSBs. In a pathbreaking attempt, He et al. recently reported a localized high-concentration electrolyte (LHCE) consisting of DME, NaFSI, and 1,1,2,2-tetrafluoroethyl 2,2,3,3-tetrafluoropropyl ether (TTE) (DME:NaFSI:TTE = 1:1.2:1) [127]. Though such high-concentration electrolytes were previously reported for oxide-based cathodes in LIBs and SIBs, it was the first time it was applied to RT-NaSBs. Even after rigorous Na plating and stripping studies, a clear and smooth Na surface was observed while using the LHCE without dendrite formation and pulverization, unlike conventional electrolytes, indicating its excellent compatibility with the Na anode. More importantly, the LHSCE could turn around the conventional dissolution–precipitation mechanism in RT-

NaSBs into a quasi-solid-state type and thereby avoid the phenomenon of NaPS shuttling, resulting in stable cycle performances for 300 cycles at a 0.1 C rate (Figure 7c).
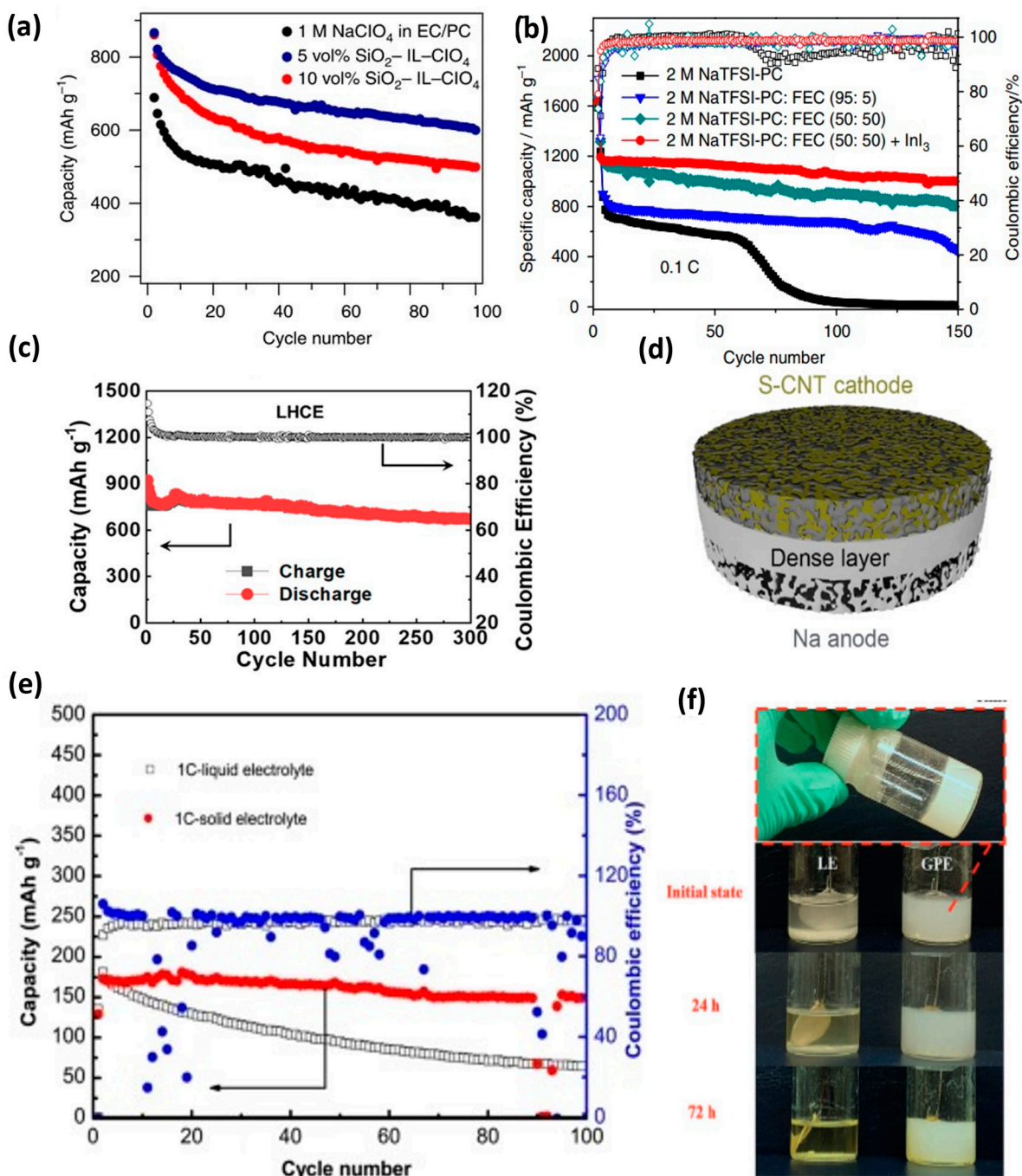

Figure 7. (**a**) Cycle performance of RT-NaSBs with a tailored SiO_2–IL–ClO_4 electrolyte with varying SiO_2 content [35]. (**b**) Comparison of cycle performances in an InI_3-embedded carbonate electrolyte with variable FEC content [17]. (**c**) Cycle performances of RT-NaSBs with a high concentration DME:NaFSI:TTE electrolyte. Reproduced with permission [127]. Copyright 2021, American Chemical Society. (**d**) Monolithic SSE with dense and porous layers. Reproduced with permission [128]. Copyright 2021, American Chemical Society. (**e**) Comparative cycle performances in RT-NaSBs with liquid and solid electrolytes [129]. (**f**) Visual observation of NaPS formation and diffusion in liquid and gel electrolytes at different aging times. Reproduced with permission [30]. Copyright 2018, Wiley.

4.3.2. Solid and Quasi-Solid Electrolytes

Research on solid-state and quasi-solid-state electrolytes has achieved tremendous growth in the past five years to realize safe rechargeable batteries. Despite the high ionic conductivity (10^{-3}–10^{-2} S cm^{-1}) and less electrolyte/electrode interfacial resistance benefitting from excellent interfacial contacts offered by the liquid electrolytes, the risk of leakage, prolific dendrite growth, and internal short-circuiting associated with them raise serious safety concerns [130]. This situation is amplified in RT-NaSBs by the additional unwarranted dissolution of NaPS species in liquid electrolytes, hindering the active sulfur utilization and adversely affecting the electrochemical performances. Given these issues, the research and development of solid-state electrolytes (SSEs) in RT-NaSBs have evolved by drawing parallels from Na-ion batteries and LSBs. The SSEs can generally be divided into inorganic solid-state electrolytes (ISSEs) and solid polymer electrolytes (SPEs). The utilization of ISSE is expected to facilitate solid-solid conversion kinetics in RT-NaSBs, avoiding PS dissolution and thereby improving the reversibility and cycle life. To verify this, fast ion-conducting materials, including sodium beta alumina (BASE), NASICON, and sulfide-based structures, have been investigated as SSEs by various research groups. It is interesting to note that research works on NASCICON-based ISSE $Na_{1+x}Zr_2P_{3-x}Si_xO_{12}$, with a three-dimensional cation transport pathway reported in the 1970s, are currently being reinvestigated for RT-NaSBs with modifications [129,131–133]. The impact of Al doping in $Na_{3.4}Zr_2(Si_{0.8}P_{0.2}O_4)_3$ structure was explored, achieving almost 4.43×10^{-3} S cm^{-1} at 50 °C for an Al content of 0.1% [128]. The strategic design of the SSE with a dense layer in between two porous layers on either side (Figure 7d) could effectively accommodate elemental sulfur and melted Na on either of the porous layers, resulting in a monolithic ASSB with excellent interfacial contact. In another study, a NASICON-based SSE $Na_{3.1}Zr_{1.95}Mg_{0.05}Si_2PO_{12}$ with a high room-temperature ionic conductivity of 3.5×10^{-3} S cm^{-1} was reported and investigated for RT-NaSBs [129]. In comparison with RT-NaSBs with liquid electrolyte (NaClO$_4$ in EC + PC) and Whatman separator, the cells with the novel NASICON SSE showed excellent capacity retention (88% after 100 cycles at 1 C rate), validating the capability of the NASICON structure in mitigating NaPS dissolution unlike that of liquid electrolytes (Figure 7e).

Sulfide-based SSEs are versatile due to their high ionic conductivities, excellent room temperature compatibility, facile synthesis methods, and ease of processibility owing to their good mechanical strength [134]. Compositing electrode materials with sulfide-based electrolytes is a simple and effective method to improve interfacial contacts. An ASSB consisting of a S/Ketjen black (KB) electrode and phosphorus sulfide (P_2S_5) or highly ionic conductive sodium thiophosphate (Na_3PS_4) revealed that nanocrystalline Na_3PS_4 was formed in situ in the S/KB-P_2S_5 electrode on electrochemically reacting with the Na anode, enhancing the interfacial contact and reversibility of RT-NaSBs [135]. In another hybrid approach, a Na_3PS_4–Na_2S–C composite electrode was investigated, wherein Na_3PS_4 was explored as both SSE and catholyte active material [136]. Additionally, a remarkably superior electrode/electrolyte interfacial contact was established for the Na_3PS_4–Na_2S–C composite electrode by introducing nanosized Na_2S, and the RT-NaSBs exhibited a promising capacity of 438.4 mAh g^{-1} after 50 cycles at 50 mA g^{-1}. A Na_2S-Na_3PS_4-CMK-3 nanocomposite prepared by a melt-casting strategy followed by annealing and in situ precipitation of active materials in mesoporous CMK-3 conductive carbon yielded a stable interface with low interfacial resistance [137]. Similar composite strategies have also been reported with phosphorus-free sulfide electrolyte, Na_3SbS_4, which possesses excellent stability in dry air. In general, liquid-phase synthesis methods are widely explored to synthesize SSEs with good interfacial contact with the cathode and electrolytes. For instance, an activated carbon-S-Na_3SbS_4 composite reported by Ando et al. exhibited high discharge capacity and reversibility [138]. The study advocated the efficacy of a liquid-phase processing technique over a solid-state one to achieve improved interfacial contact. In a modified approach, nano-scaled ion conduction pathways were developed in situ within the S-Na_3SbS_4-C cathode by a liquid-phase synthesis followed by mechanical milling [139].

S-Na$_3$SbS$_4$-C/Na cells with ultra-high cathode loading of 6.34 and 12.74 mg cm^{-5} could achieve remarkable discharge capacities of 742.9 and 465.6 mAh g^{-1} at 100 mA g^{-1}, indicating excellent prospects for scaleup. Doping NaI into Na$_3$SbS$_4$ has been reported as a practical approach to enhancing ionic conductivity by incorporating highly polarizable I^{-} ions [140]. Wan et al. implemented the concept in RT-NaSBs and achieved in situ formation of ionic as well as electronic conduction pathways in a hybrid S cathode structure combing 0.9 Na$_3$SbS$_4$ 0.1 NaI (1.01 × 10^{-3} S cm^{-1} at 30 °C) with Fe$_3$S$_4$ and S [141]. Similarly, an Fe$_3$S$_4$@S@0.9 Na$_3$SbS$_4$ 0.1 NaI composite prepared via a wet mechano-chemical milling process avoiding an additional sintering process, displayed excellent rate capability (952.4 and 445.6 mAh g^{-1} at 50 and 500 mA g^{-1}, respectively) when coupled with a Na anode.

A Na-ion conducting PEO-based SPE was reported by Ge et al., incorporating NaCF$_3$SO$_3$ as sodium salt and MIL-53(Al) as filler [142]. High ionic conductivities (6.87 × 10^{-5} S cm^{-1} at 60 °C) were achieved with 3.24 wt% MIL-53 (Al) and simultaneously adjusting the mole ratio of EO (ethylene oxide of PEO): Na (sodium ion of NaCF$_3$SO$_3$) as 20:1. Similarly, PEO–NaFSI–1% TiO$_2$ displayed a high ionic conductivity of 4.89 × 10^{-4} S cm^{-1} at 60 °C with excellent electrochemical and thermal stability [143]. When coupled with a S/CPAN (carbonized polyacrylonitrile) cathode, the ASSB exhibited remarkable cyclability, retaining 710 mAh g$_{(s)}$$^{-1}$ even after 100 cycles.

Though SSEs have demonstrated promising electrochemical performances in RT-NaSBs, it is essential to enhance the cycle performance to meet the benchmarks of commercialization. The low ionic conductivity at room temperature arising from high grain boundary resistance coupled with the sluggish Na ion transport in SSEs remains a major obstacle [144]. Adding minimal amounts of liquid electrolytes to SSEs leads to the formation of quasi-solid-state electrolytes (QSSEs), which is a practical approach to counteract the low ionic conductivity of SSEs and improve the interfacial contact between the electrolyte and electrode/anode. The semi-liquid-like property of QSSEs offers rapid ion transport, though the intrinsic safety is partly compromised by the addition of liquid components. The initial reports on QSSEs in RT-Na-S batteries were regarding polymer-based gel electrolytes (GPEs); however, the electrochemical performances were not satisfactory. In one of the pioneering works, Park et al. reported a Poly(vinylidene fluoride-hexafluoropropylene) (PVDF-HFP)-based GPE with a high sodium ion conductivity (5.1 × 10^{-4} S cm^{-1} at 25 °C), synthesized utilizing TEGDME as plasticizer and NaCF$_3$SO$_3$ as the sodium salt [20]. A drastic deterioration in discharge capacity was observed with cycling, and the cells could not be cycled beyond 20 cycles. Later, short-term cycling of PVdF-HFP-based GPE prepared with TEGDME plasticizer and NaCF$_3$SO$_3$ salt was demonstrated by Kim et al., which also revealed the prospects of QSSE in RT-NaSBs [118].

Apart from tuning the crystallinity of polymers and incorporating suitable fillers and plasticizers, novel approaches such as applying rational coatings on the surface of PEs have proven to be highly beneficial. In that aspect, adding varying amounts of SiO$_2$ nanoparticles as filler in PVdF-HFP, immobilized with NaCF$_3$SO$_3$ in a carbonate electrolyte (EC: PC; 1:1, *v/v*), was also investigated [145]. Though the PVdF-HFP–EC: PC (1:1 *v/v*)–NaCF$_3$SO$_3$ dispersed with ~3 wt.% of SiO$_2$ displayed a high ionic conductivity (4.1 × 10^{-3} S cm^{-1}), the Na transference number of the GPE with 15 wt.% SiO$_2$ was higher. However, the cycle performance of RT-NaSBs was not satisfactory. GPEs with conventional carbonate-free electrolytes have also been investigated extensively from earlier on. In such an attempt, NaCF$_3$SO$_3$ dissolved in an ionic liquid (1-ethyl 3-methyl imidazolium trifluoro-methane sulfonate; EMITf) was entrapped in PVdF-HFP, and the GPE was prepared by a solution casting method [146]. This concept was later applied for RT-NaSBs by the same group, employing an EMITf/PVdF-HFP ratio of 4:1 *w/w* [147]. Good capacity retention (98.2% at 0.2 C after 200 cycles) was achieved for an RT-NaSBs employing a gel PVDF-HFP-based GPE with nanosized SiO$_2$ fillers entrapped with NaPF$_6$/diethylene glycol dimethyl ether (DEGDME) exhibiting a high Na$^+$ conductivity of 0.5 mS cm^{-1} [148]. Such approaches can improve the reversibility of RT-NaSBs by effectively mitigating the precipitation of inactive S at the electrode–electrolyte interface. A quasi-solid-state RT-NaSB was reported

using a crosslinked PETEA-tris [2-(acryloyloxy)ethyl]isocyanurate (PETEA-THEICTA)-based GPE via radical polymerization [30]. Figure 7f shows the visual observation of NaPS formation and diffusion in liquid and gel electrolytes at different aging times. The high ionic conductivity GPE formed in situ displayed excellent compatibility with the Na anode providing a stable Na metal interface while simultaneously immobilizing the NaPS species, unlike the case of liquid electrolytes.

Coating polymers on SSE can enable quasi-solid-state behavior when coupled with a few drops of liquid electrolyte. Exploring that viewpoint, a NASCICON-type $Na_3Zr_2Si_2PO_{12}$ SSE with a polymer coating with intrinsic nanoporosity (PIN) on the anode side was developed with improved interfacial contact with Na [149]. The Na‖PIN-$Na_3Zr_2Si_2PO_{12}$‖CNF/S cell fabricated with a few additional drops of $NaClO_4$/TEGDME exhibited cycle performances (550 mA h g^{-1} at 0.2 C after 100 cycles) far superior to that of cells with conventional Celgard and $NaClO_4$/TEGDME electrolyte (Figure 8a).

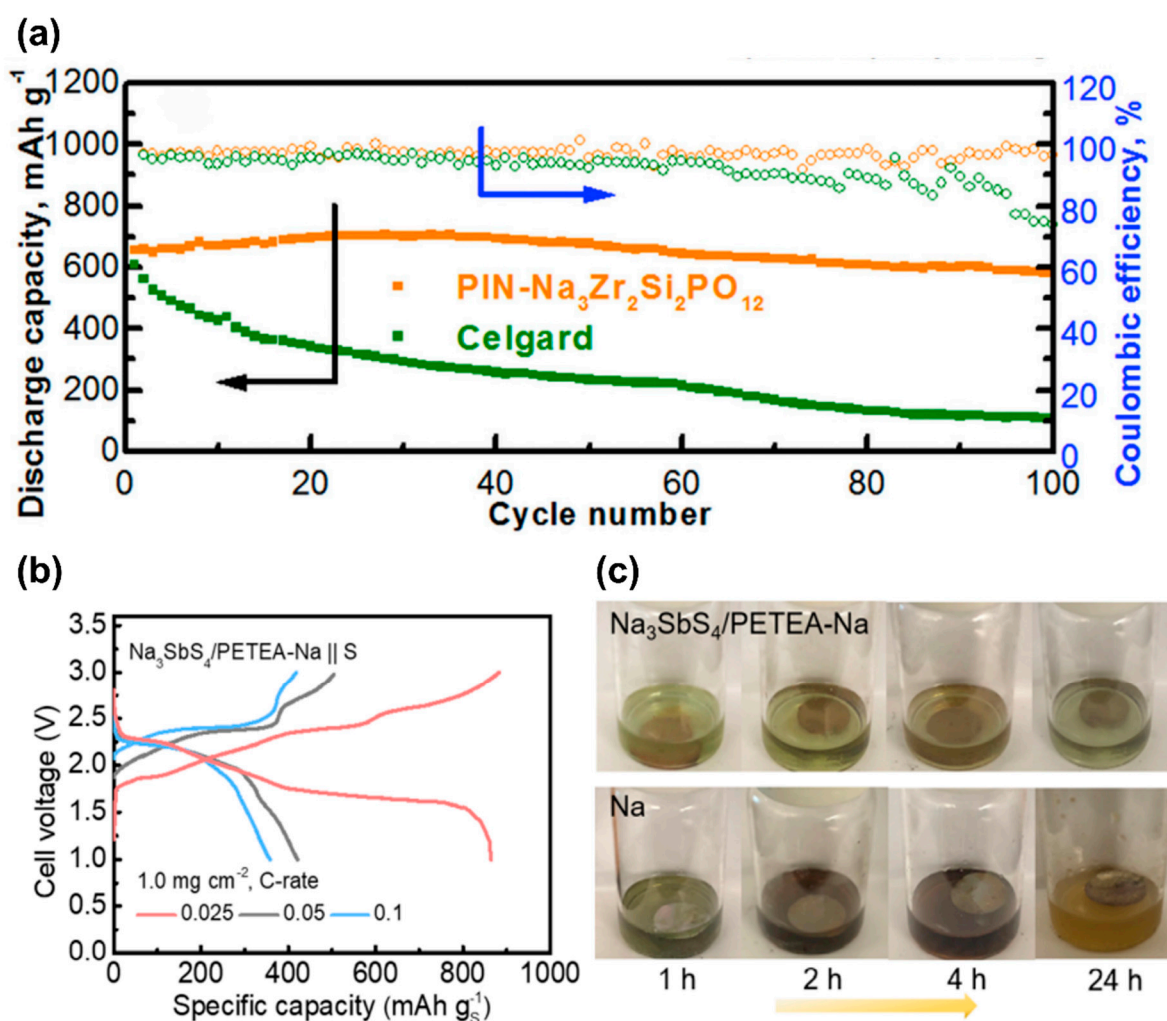**Figure 8.** (**a**) Cycle performance of Na‖PIN-$Na_3Zr_2Si_2PO_{12}$‖CNF/S cell. Reproduced with permission [149]. Copyright 2019, Cell Press. (**b**) Voltage profiles of Na_3SbS_4/PETEA-Na‖S cells at various current rates, and (**c**) visual observation of changes in Na_3SbS_4/PETEA-Na and bare Na soaked in the liquid electrolyte containing sulfur powder. Reproduced with permission [150]. Copyright 2021, American Chemical Society.

Kim et al. employed a hybrid electrolyte consisting of Na-BASE and $NaCF_3SO_3$/TEGDME ether electrolyte solution [151]. The study achieved a high discharge capacity of 855 mA h g^{-1} by employing a porous S/C cathode with the hybrid SSE; however, the capacity de-

graded considerably with cycling. Interestingly, the post-cycling analysis of the cathode revealed the absence of pulverization and signs of NaPS dissolution, respectively. The white surface of the SSE after the 104th charge indicated that the NaPS dissolution was completely avoided as the dissolved higher-order NaPS species tend to leave brown coloration on separators. Further investigations by examining the BASE at different points of the charge/discharge cycle revealed that the dissolution of NaPS could be controlled by regulating the molar concentration of active S, specifically the S to TEGDME ratio in the cell [152]. Recently, a novel hybrid electrolyte was reported by in situ cross-linking sulfide based Na_3SbS_4 electrolyte with a flexible gel polymer to improve the compatibility of Na_3SbS_4 with the Na anode and avoid parasitic deposition of Na [150]. The spontaneous cross-linking ability of Na_3SbS_4 with pentaerythritol tetraacrylate (PETEA) monomer beyond 150 °C was explored to prepare gel-like hybrid thin films (≤30 μm). Prototype Na_3SbS_4-PETEA-Na∥S cells demonstrated good reversibility (Figure 8b) and cyclability up to 90 cycles. The visual observation of changes in Na_3SbS_4/PETEA-Na and bare Na soaked in the liquid electrolyte containing sulfur powder revealed no observable changes occurring with the hybrid solid electrolyte, unlike that of bare Na, indicating the inability of the liquid electrolyte to penetrate through Na_3SbS_4/PETEA-Na and to react with metallic Na (Figure 8c). This indicates the effectiveness of Na_3SbS_4/PETEA-Na in blocking NaPS diffusion to the anode side.

4.4. Interfacial Engineered Na Anode

The excellent electrical conductivity and strong reducibility make Na metal an ideal anode material, similar to Li [153]. Despite these advantages, the sluggish reaction kinetics of Na and the unwarranted side reactions with electrolytes result in prolific Na dendrite growth that adversely affects the lifespan of cells, simultaneously raising severe safety hazards. Thus, the interfacial engineering of the Na anode has emerged as a hot topic in rechargeable batteries [154,155]. Coating a thin protective film on the surface of the Na anode to form an artificial SEI is a widely adopted strategy to inhibit the formation of Na dendrites. For instance, employing atomic layer deposition (ALD) and molecular layer deposition (MLD) techniques (Figure 9) has been beneficial in achieving an ultra-thin coating layer on the Na anode [156,157]. Such strategies have been demonstrated to immensely stabilize the Na anode surface, reducing the polarization and enhancing the cycle life of batteries. Further, such passivating layers (SEI film) can also be achieved in situ by employing suitable electrolyte formulations, additives, and cycling strategies, as detailed in Section 4.3.1.
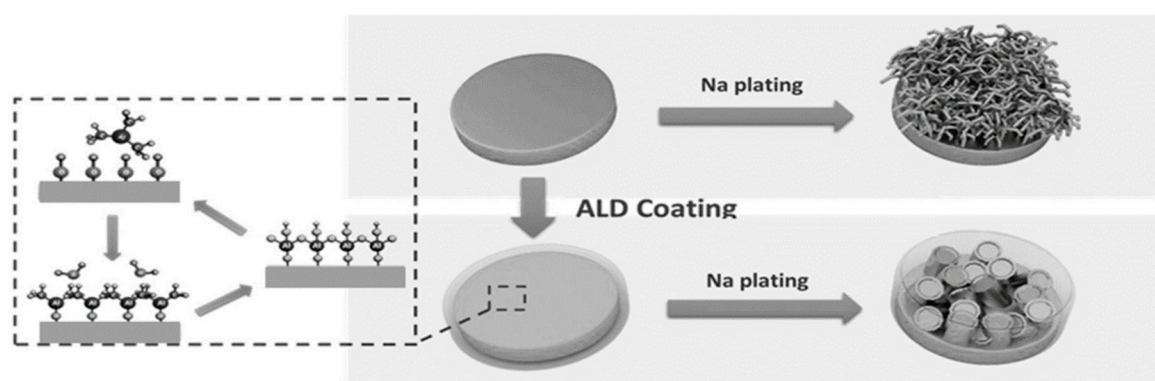

Figure 9. Schematic representation of Na anode protection strategy employing atomic layer deposition. Reproduced with permission [156]. Copyright 2017, Wiley.

The cell chemistry of RT-NaSBs involving NaPS generation, dissolution, and migration to the anode side, where it reduces to lower-order NaPS, warrants strategic measures to protect the interface of metallic Na. Vipin et al. fabricated an artificial metal-alloy interphase (MAI) in an anode (Figure 10a) consisting of Na-Sn alloy, employing a solid-vapor reaction

of Na metal with tin tetrachloride vapors [158]. The developed MAI could facilitate reversible Na deposition at current densities as high as 5–7 mA cm^{-2} in symmetric cells (Figure 10b) and exhibited good cyclability (500 cycles) when employed in RT-NaSBs (Figure 10c). Recently, a tailored biphasic interface (BPI) was designed for the Na anode utilizing NaOH and NaNH$_2$ distinctly rendering stiffness and ductility, respectively, to facilitate a dendrite-free Na surface after cycling (Figure 10d) [159]. The low diffusion barrier of Na$^+$ species at this unique interface enabled excellent reversible Na deposition even at extremely high current densities (up to 50 mA cm^{-2}) in Na symmetric cells. RT-NaSBs with BPI exhibited stable and reversible cycling over 500 cycles (Figure 10e,f).
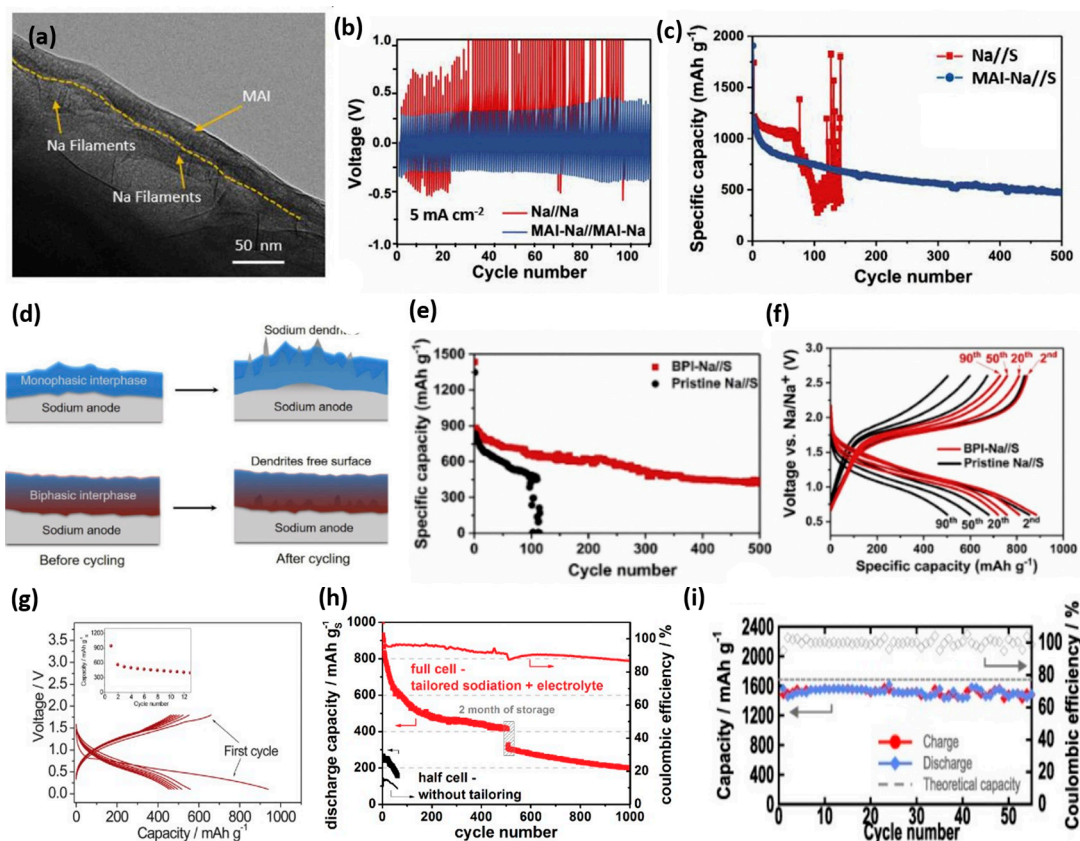

Figure 10. (**a**) Cryo-TEM micrographs of the as-deposited Na with MAI, (**b**) galvanostatic stripping/plating test of Na symmetric cells with and without MAI at 5 mA cm^{-2}, and (**c**) cycle performance of RT-NaSBs with and without MAI. Reproduced with permission [158]. Copyright 2020, Elsevier. (**d**) Schematic illustration of the effect of cycling on Na anode with and without BPI (**e**) cycle performance and (**f**) voltage profiles of RT-NaSBs with and without BPI. Reproduced with permission [159]. Copyright 2020, Cell Press. Voltage profiles of (**g**) Na–Sn–C/TEGDME$_4$-NaCF$_3$SO$_3$/HCS–S full cell. Reproduced with permission [119]. Copyright 2013, Royal Society of Chemistry. (**h**) Comparative cycle performance of RT-NaS cells with 1 M NaClO$_4$ 0.2 M Na$_2$S/P$_2$S$_5$ in TEGDME | Na anode (black lines) and a hard carbon anode sodiated in 1 M NaPF$_6$ in DEC: EC + FEC (6:4 + 1% vol.) (red lines). Reproduced with permission [124]. Copyright 2016, Wiley. (**i**) ASSB using an S-MSP20-Na$_3$SbS$_4$ composite electrode. Reproduced with permission [138].

Generally, integrated full-cell architectures employing engineered S cathodes and modified anode configurations are found to mitigate the NaPS shuttle effect, effectively avoiding the internal shorting of cells, and facilitating extended long-cycle performances. Employing sodium metal-free anodes such as hard carbon (HC), Si, and Sn can render excellent safety and durability for cells considering practical applications [103]. Such pre-sodiated anodes have been investigated in RT-NaSBs by various groups. The hollow C/S composite prepared from a spherical SiO$_2$ template with almost 60% S loading in

combination with a pre-sodiated nanostructured Sn–C anode and an ether electrolyte exhibited a reversible capacity of 550 mAh g^{-1} and an energy density of 550 W h kg^{-1} at 0.1 C rate, with a low operating voltage of 1 V (See Figure 10g) [119]. Kohl et al. demonstrated RT-NaS full cells with an HC anode and a porous C/S composite for the first time, with a high discharge capacity of 980 mA h g^{-1} [124]. Compared with the cells with metallic Na anode, the cells with pre-sodiated HC anodes exhibited superior cycle performances (Figure 10h). However, major capacity degradation was observed in the initial 200 cycles, though the cell could run up to 1000 cycles. Followingly, RT-NaSBs with pre-sodiated HC anode reported by Pampel et al. on pouch cell level, exhibited stable cycling over 1000 cycles [160].

Despite the successful implementation of HC anodes at the pouch cell level, the HC anode is not a preferred choice, considering the complications associated with pre-sodiation and its translation to a commercial level. In this context, Na$_2$S has gained wide popularity as an alternate cathode that already possesses Na, which does not require pre-sodiation when coupled with HC anodes [161]. The first RT-NaS full cell with a Na$_2$S/C cathode and an HC anode demonstrated with a precisely optimized electrolyte containing FEC and, by following specified charging procedures in the initial cycles, delivered 350 mAh g^{-1} based on the S mass at 0.2 C rate [162]. Exploring alternative anodes to Na, a Na$_3$Sb alloying anode coated with Na$_3$PS$_4$ SE coupled with an activated carbon-S-Na$_3$SbS$_4$ composite was developed recently by Ando et al. [138]. ASSBs with this alloying anode exhibited a remarkable discharge capacity of 1560 mAhg^{-1} (93% of the theoretical capacity), for over 50 cycles at a current density of 0.064 mA cm^{-2} (Figure 10i). Fostering similar approaches by investigating the pitfalls of such integrated cells and redesigning solutions for them are critical in realizing practical RT-NaSBs in the near future.

5. Conclusions and Future Perspectives

RT-NaSBs are a promising alternative for next-generation energy storage after LSBs, considering the high achievable capacity and energy density and low cost. With the advantage of exhibiting similar electrochemical behavior to LSBs, RT-Na-S batteries offer immense opportunities for sustainable grid-scale energy storage. However, apart from the cost-effectiveness, environmental benignity, and ease of translation of technology from LSBs, RT-NaSB research is still in its infancy, and there are severe challenges that need to be addressed to facilitate the commercialization of this system. Henceforth, this review is a summary of the state-of-the-art RT-NaSBs, electrode and interfacial engineering strategies adopted for PS adsorption, and mitigation in RT-NaSB research to date.

Electrode engineering: As discussed, the uncontrolled NaPS shuttling in the electrolyte hinders the development of high-performance RT-NaSBs. The strategies to improve the performance of RT-NaSBs require adequate addressing by carefully analyzing the contributions and challenges from various cell components in terms of polysulfide trapping. The main strategies to inhibit/adsorb the polysulfide species are by confining them to the cathode, separator, interlayer, and electrolyte. The strategy of employing carbonaceous hosts for loading S is an inexpensive method. However, the limited S content (>50%) in them is not favorable for practical application. To improve the S content in the cathode beyond >70%, carbon nanoarchitecture with tunable multimodal porosities should be explored. Covalently bonded S/C composites also suffer from low S content owing to the inability to establish S-C covalent bonds beyond a limit. Designing suitable S-containing electrochemically active materials with high capacities and synthesizing them in situ with S/C composites can be beneficial to push the boundaries of S loading in electrodes. NaPS adsorption/trapping in RT-NaSBs demands a combination of physical and chemical adsorption strategies involving integrated cathode architectures with high surface and multimodal porosities embedding suitable polar materials and catalytic redox mediators. Incorporating transition metal oxides, sulfides, and selenides can improve the reaction kinetics of NaPS conversion in RT-NaSBs, enabling long-term cyclability while elevating the S content in the electrode without compromising electrochemical performances. The main challenge

in designing such efficient S electrodes is to engineer homogeneously dispersed adsorptive/catalytic sites in the cathode. Apart from that, the content of polar materials and electrocatalysts should be carefully assessed, without sacrificing the overall energy density of the system by adding to the dead weight. Additionally, the specific role of various catalytic redox mediators in boosting the redox kinetics of NaPS conversion reaction needs to be studied in-depth to formulate and finetune the electrochemical reactions via electrochemical studies involving CV and galvanostatic intermittent titration (GITT). Surface chemical characterizations such as Raman and XPS can also aid in understanding the contribution of such catalytic mediators in facilitating rapid NaPS conversion/reconversions. Overall, strategically confined electrode architectures exploiting the principles of physical and chemical adsorption along with good electrolyte compatibility can enable highly reversible RT-NaSBs with prolonged cycle life. However, the scale-up of such hybrid electrodes with electrocatalysts requires adequate engineering and socio-economic analysis to satisfy the commercialization targets.

Interfacial engineering: Optimizing electrolytes is another major hurdle to achieving RT-NaSBs with good reversibility. The ready dissolution of NaPS species in ether electrolytes and the inhibition of PS generation in carbonate electrolytes demand clear mechanistic insights into the reaction mechanisms to unravel the influence of electrode/electrolyte and electrolyte/anode interfaces. Single electrolyte additives such as FEC as well as a combination of Na_2S and P_2S_5 are proven to improve the compatibility of electrolytes with both electrodes and the anode. However, their large-scale utilization is never feasible due to the high costs. Additionally, the integration of solid-state and quasi-solid-state electrolytes can boost the reversibility and long-term cycle life of RT-NaSBs though the Na-ion conductivity of such systems, which is significantly lower than that of conventional liquid electrolytes. Comprehensive study of interfacial changes during cycling in such systems can be beneficial. Additionally, Na anodes are highly reactive and are prone to unwanted parasitic reactions when in contact with liquid electrolytes. The inefficient Na^+ transport and Na^+ concentration polarization lead to non-uniform accumulation of Na^+ charges contributing to dendritic Na growth and affecting the safe operation of cells. Mitigating Na dendritic growth during extended cycling is yet another major hurdle to achieving safe RT-NaSBs with long-term cyclability. Though various Na anode protection strategies are being explored, it is essential to undertake in-depth studies to understand the SEI layer formation and its chemical components to clearly outline the role of interfaces. Additionally, the irreversible loss of Na via the formation of an SEI layer and the associated low CEs are hindrances to achieving good cycle performances. In that regard, designing solid-state electrolytes and tunable SEI layers can simultaneously alleviate the polysulfide shuttle phenomenon while enabling unified and rapid Na^+ flux in the system. Exploring Na metal-free anodes have brought RT-NaSBs one step closer to commercial standards. However, tailoring electrode/electrolyte/anode interfaces in RT-NaS full batteries to maximize the reversibility and cycle life calls for extensive studies using advanced characterizations.

Cell development: Exploiting the benefits of low-cost raw materials and the achievable high energy density of RT-NaSBs, electrode designs that can accommodate high S loadings (typically ≥ 5 mg cm^{-2}) need to be extensively investigated to evaluate the commercial applications of this system. Novel manufacturing techniques such as 3D printing and powder technology facilitate the flexibility to incorporate complex designs and bring about cost effectiveness. Additionally, the good prospects for scale-up offered by these techniques make them suitable to prepare high-loading electrodes on a large scale. In addition, achieving a low E/S ratio is essential to avoid parasitic reactions that arise due to the contact of S species with the electrolyte and thereby reduce the NaPS dissolution. A low E/S ratio also contributes to the improvement of the overall energy density of the cell. Engineering novel solid electrolytes with good Na compatibility would be highly significant. The mitigation of PS shuttling in large-format cells is challenging and requires extensive investigation and optimization. The extension of S-incorporated cathode structures to

various cell architectures such as pouch cells and cylindrical cells can be beneficial to understand the true performances.

Finally, it is anticipated that high reversible capacity and long-term cyclability can be achieved for RT-NaSBs by employing simple and low-cost defense pathways for NaPS trapping and by rationally integrating engineered S cathodes, modified functional separators, interlayers, suitable electrolyte systems, and safe Na-free anodes. Such sustainable attempts can draw RT-NaSBs closer to commercialization and scale-up in view of potential large-scale applications.

References

1. Manthiram, A.; Fu, Y.; Chung, S.H.; Zu, C.; Su, Y.S. Rechargeable lithium-sulfur batteries. *Chem. Rev.* **2014**, *114*, 11751–11787. [CrossRef] [PubMed]
2. Su, Y.S.; Fu, Y.; Cochell, T.; Manthiram, A. A strategic approach to recharging lithium-sulphur batteries for long cycle life. *Nat. Commun.* **2013**, *4*, 2985. [CrossRef] [PubMed]
3. Dunn, B.; Kamath, H.; Tarascon, J.-M. Electrical Energy Storage for the Grid: A Battery of Choices. *Science* **2011**, *334*, 928–935. [CrossRef]
4. Li, M.; Lu, J.; Chen, Z.; Amine, K. 30 Years of Lithium-Ion Batteries. *Adv Mater.* **2018**, *30*, e1800561. [CrossRef]
5. Albertus, P.; Babinec, S.; Litzelman, S.; Newman, A. Status and challenges in enabling the lithium metal electrode for high-energy and low-cost rechargeable batteries. *Nat. Energy* **2017**, *3*, 16–21. [CrossRef]
6. Haridas, A.K.; Sadan, M.K.; Kim, H.; Heo, J.; Kim, S.S.; Choi, C.H.; Jung, H.Y.; Ahn, H.J.; Ahn, J.H. Realizing High-Performance Li/Na-Ion Half/Full Batteries via the Synergistic Coupling of Nano-Iron Sulfide and S-doped Graphene. *ChemSusChem* **2021**, *14*, 1936–1947. [CrossRef]
7. Zhou, G.; Chen, H.; Cui, Y. Formulating energy density for designing practical lithium–sulfur batteries. *Nat. Energy* **2022**, *7*, 312–319. [CrossRef]
8. Liang, Z.; Shen, J.; Xu, X.; Li, F.; Liu, J.; Yuan, B.; Yu, Y.; Zhu, M. Advances in the Development of Single-Atom Catalysts for High-Energy-Density Lithium-Sulfur Batteries. *Adv. Mater.* **2022**, *34*, e2200102. [CrossRef]
9. Peng, H.-J.; Huang, J.-Q.; Cheng, X.-B.; Zhang, Q.; Peng, H.-J.; Huang, J.-Q.; Cheng, X.-B.; Zhang, Q. Lithium-Sulfur Batteries: Review on High-Loading and High-Energy Lithium-Sulfur Batteries (Adv. Energy Mater. 24/2017). *Adv. Energy Mater.* **2017**, *7*, 1700260. [CrossRef]
10. Yang, C.; Li, P.; Yu, J.; Zhao, L.-D.; Kong, L. Approaching energy-dense and cost-effective lithium–sulfur batteries: From materials chemistry and price considerations. *Energy* **2020**, *201*, 117718. [CrossRef]
11. Lim, W.; Kim, S.; Jo, C.; Lee, J. A Comprehensive Review of Materials with Catalytic Effects in Li–S Batteries: Enhanced Redox Kinetics. *Angew. Chem.* **2019**, *131*, 18920–18931. [CrossRef]
12. Bruce, P.G.; Freunberger, S.A.; Hardwick, L.J.; Tarascon, J.M. Li-O$_2$ and Li-S batteries with high energy storage. *Nat. Mater.* **2011**, *11*, 19–29. [CrossRef] [PubMed]
13. Jin, F.; Wang, B.; Wang, J.; Wang, Y.; Ning, Y.; Yang, J.; Zhang, Z.; Liu, P.; Zhou, Y.; Wang, D.; et al. Boosting electrochemical kinetics of S cathodes for room temperature Na/S batteries. *Matter* **2021**, *4*, 1768–1800. [CrossRef]
14. Ye, X.; Ruan, J.; Pang, Y.; Yang, J.; Liu, Y.; Huang, Y.; Zheng, S. Enabling a Stable Room-Temperature Sodium–Sulfur Battery Cathode by Building Heterostructures in Multichannel Carbon Fibers. *ACS Nano* **2021**, *15*, 5639–5648. [CrossRef] [PubMed]
15. Zhang, S.; Yao, Y.; Yu, Y. Frontiers for Room-Temperature Sodium–Sulfur Batteries. *ACS Energy Lett.* **2021**, *6*, 529–536. [CrossRef]
16. Yu, Y.Y.-F.; Kummer, J.T. Ion exchange properties of and rates of ionic diffusion in beta-alumina. *J. Inorg. Nucl. Chem.* **1967**, *29*, 2453–2475.
17. Xu, X.; Zhou, D.; Qin, X.; Lin, K.; Kang, F.; Li, B.; Shanmukaraj, D.; Rojo, T.; Armand, M.; Wang, G. A room-temperature sodium-sulfur battery with high capacity and stable cycling performance. *Nat. Commun.* **2018**, *9*, 3870. [CrossRef] [PubMed]
18. Wang, Y.; Zhang, B.; Lai, W.; Xu, Y.; Chou, S.; Liu, H.; Dou, S. Room-Temperature Sodium-Sulfur Batteries: A Comprehensive Review on Research Progress and Cell Chemistry. *Adv. Energy Mater.* **2017**, *7*, 1602829. [CrossRef]

19. Wen, Z.; Cao, J.; Gu, Z.; Xu, X.; Zhang, F.; Lin, Z. Research on sodium sulfur battery for energy storage. *Solid State Ionics* **2008**, *179*, 1697–1701. [CrossRef]

20. Park, C.-W.; Ahn, J.-H.; Ryu, H.-S.; Kim, K.-W.; Ahn, H.-J. Room-Temperature Solid-State Sodium/Sulfur Battery. *Electrochem. Solid-State Lett.* **2006**, *9*, A123–A125. [CrossRef]

21. Eng, A.Y.S.; Kumar, V.; Zhang, Y.; Luo, J.; Wang, W.; Sun, Y.; Li, W.; Seh, Z.W. Room-Temperature Sodium–Sulfur Batteries and Beyond: Realizing Practical High Energy Systems through Anode, Cathode, and Electrolyte Engineering. *Adv. Energy Mater.* **2021**, *11*, 2003493. [CrossRef]

22. Qiang, Z.; Chen, Y.-M.; Xia, Y.; Liang, W.; Zhu, Y.; Vogt, B.D. Ultra-long cycle life, low-cost room temperature sodium-sulfur batteries enabled by highly doped (N,S) nanoporous carbons. *Nano Energy* **2017**, *32*, 59–66. [CrossRef]

23. Manthiram, A.; Yu, X. Ambient Temperature Sodium-Sulfur Batteries. *Small* **2015**, *11*, 2108–2114. [CrossRef] [PubMed]

24. Yu, X.; Manthiram, A. Capacity Enhancement and Discharge Mechanisms of Room-Temperature Sodium-Sulfur Batteries. *ChemElectroChem* **2014**, *1*, 1275–1280. [CrossRef]

25. Ryu, H.; Kim, T.; Kim, K.; Ahn, J.-H.; Nam, T.; Wang, G.; Ahn, H.-J. Discharge reaction mechanism of room-temperature sodium–sulfur battery with tetra ethylene glycol dimethyl ether liquid electrolyte. *J. Power Sources* **2011**, *196*, 5186–5190. [CrossRef]

26. Wang, N.; Wang, Y.; Bai, Z.; Fang, Z.; Zhang, X.; Xu, Z.; Ding, Y.; Xu, X.; Du, Y.; Dou, S.; et al. High-performance room-temperature sodium–sulfur battery enabled by electrocatalytic sodium polysulfides full conversion. *Energy Environ. Sci.* **2020**, *13*, 562–570. [CrossRef]

27. Shim, J.; Striebel, K.A.; Cairns, E.J. The Lithium/Sulfur Rechargeable Cell. *J. Electrochem. Soc.* **2002**, *149*, A1321. [CrossRef]

28. Bauer, I.; Kohl, M.; Althues, H.; Kaskel, S. Shuttle suppression in room temperature sodium–sulfur batteries using ion selective polymer membranes. *Chem. Commun.* **2014**, *50*, 3208–3210. [CrossRef]

29. Yang, Z.; Xiao, R.; Zhang, X.; Wang, X.; Zhang, D.; Sun, Z.; Li, F. Role of Catalytic Materials on Conversion of Sulfur Species for Room Temperature Sodium–Sulfur Battery. *Energy Environ. Mater.* **2021**, *5*, 693–710. [CrossRef]

30. Zhou, D.; Chen, Y.; Li, B.; Fan, H.; Cheng, F.; Shanmukaraj, D.; Rojo, T.; Armand, M.; Wang, G. A Stable Quasi-Solid-State Sodium-Sulfur Battery. *Angew. Chem. Int. Ed. Engl.* **2018**, *57*, 10168–10172. [CrossRef]

31. Soni, C.B.; Sungjemmenla; Vineeth, S.K.; Kumar, V. Challenges in regulating interfacial-chemistry of the sodium-metal anode for room-temperature sodium-sulfur batteries. *Energy Storage* **2021**, *4*, e264. [CrossRef]

32. Xin, S.; Yin, Y.-X.; Guo, Y.-G.; Wan, L.-J. A High-Energy Room-Temperature Sodium-Sulfur Battery. *Adv. Mater.* **2014**, *26*, 1261–1265. [CrossRef] [PubMed]

33. Hao, Y.; Li, X.; Sun, X.; Wang, C. Nitrogen-Doped Graphene Nanosheets/S Composites as Cathode in Room-Temperature Sodium-Sulfur Batteries. *ChemistrySelect* **2017**, *2*, 9425–9432. [CrossRef]

34. Lu, Q.; Wang, X.; Cao, J.; Chen, C.; Chen, K.; Zhao, Z.; Niu, Z.; Chen, J. Freestanding carbon fiber cloth/sulfur composites for flexible room-temperature sodium-sulfur batteries. *Energy Storage Mater.* **2017**, *8*, 77–84. [CrossRef]

35. Wei, S.; Xu, S.; Agrawral, A.; Choudhury, S.; Lu, Y.; Tu, Z.; Ma, L.; Archer, L.A. A stable room-temperature sodium–sulfur battery. *Nat. Commun.* **2016**, *7*, 11722. [CrossRef]

36. Chen, Y.-M.; Liang, W.; Li, S.; Zou, F.; Bhaway, S.M.; Qiang, Z.; Gao, M.; Vogt, B.D.; Zhu, Y. A nitrogen doped carbonized metal–organic framework for high stability room temperature sodium–sulfur batteries. *J. Mater. Chem. A* **2016**, *4*, 12471–12478. [CrossRef]

37. Guo, Q.; Li, S.; Liu, X.; Lu, H.; Chang, X.; Zhang, H.; Zhu, X.; Xia, Q.; Yan, C.; Xia, H. Ultrastable Sodium–Sulfur Batteries without Polysulfides Formation Using Slit Ultramicropore Carbon Carrier. *Adv. Sci.* **2020**, *7*, 1903246. [CrossRef] [PubMed]

38. Jana, M.; Xu, R.; Cheng, X.-B.; Yeon, J.S.; Park, J.M.; Huang, J.-Q.; Zhang, Q.; Park, H.S. Rational design of two-dimensional nanomaterials for lithium–sulfur batteries. *Energy Environ. Sci.* **2019**, *13*, 1049–1075. [CrossRef]

39. Zuo, P.; Zhang, W.; Hua, J.; Ma, Y.; Du, C.; Cheng, X.; Gao, Y.; Yin, G. A Novel One-dimensional Reduced Graphene Oxide/Sulfur Nanoscroll Material and its Application in Lithium Sulfur Batteries. *Electrochim. Acta* **2016**, *222*, 1861–1869. [CrossRef]

40. Pei, F.; Lin, L.; Ou, D.; Zheng, Z.; Mo, S.; Fang, X.; Zheng, N. Self-supporting sulfur cathodes enabled by two-dimensional carbon yolk-shell nanosheets for high-energy-density lithium-sulfur batteries. *Nat. Commun.* **2017**, *8*, 482. [CrossRef]

41. Dutta, S.; Bhaumik, A.; Wu, K.C.W. Hierarchically porous carbon derived from polymers and biomass: Effect of interconnected pores on energy applications. *Energy Environ. Sci.* **2014**, *7*, 3574–3592. [CrossRef]

42. He, J.; Chen, Y.; Li, P.; Fu, F.; Wang, Z.; Zhang, W. Three-dimensional CNT/graphene–sulfur hybrid sponges with high sulfur loading as superior-capacity cathodes for lithium–sulfur batteries. *J. Mater. Chem. A* **2015**, *3*, 18605–18610. [CrossRef]

43. Wang, Y.-X.; Yang, J.; Lai, W.; Chou, S.-L.; Gu, Q.-F.; Liu, H.K.; Zhao, D.; Dou, S.X. Achieving High-Performance Room-Temperature Sodium–Sulfur Batteries With S@Interconnected Mesoporous Carbon Hollow Nanospheres. *J. Am. Chem. Soc.* **2016**, *138*, 16576–16579. [CrossRef]

44. Carter, R.; Oakes, L.; Douglas, A.; Muralidharan, N.; Cohn, A.P.; Pint, C.L. A Sugar-Derived Room-Temperature Sodium Sulfur Battery with Long Term Cycling Stability. *Nano Lett.* **2017**, *17*, 1863–1869. [CrossRef] [PubMed]

45. Zhang, L.; Zhang, B.; Dou, Y.; Wang, Y.; Al-Mamun, M.; Hu, X.; Liu, H. Self-Assembling Hollow Carbon Nanobeads into Double-Shell Microspheres as a Hierarchical Sulfur Host for Sustainable Room-Temperature Sodium–Sulfur Batteries. *ACS Appl. Mater. Interfaces* **2018**, *10*, 20422–20428. [CrossRef]

46. Chen, W.; Wan, M.; Liu, Q.; Xiong, X.; Yu, F.; Huang, Y. Heteroatom-Doped Carbon Materials: Synthesis, Mechanism, and Application for Sodium-Ion Batteries. *Small Methods* **2018**, *3*, 180032. [CrossRef]

47. Asefa, T.; Huang, X. Heteroatom-Doped Carbon Materials for Electrocatalysis. *Chemistry* **2017**, *23*, 10703–10713. [CrossRef]
48. Cui, H.; Guo, Y.; Guo, L.; Wang, L.; Zhou, Z.; Peng, Z. Heteroatom-doped carbon materials and their composites as electrocatalysts for CO2 reduction. *J. Mater. Chem. A* **2018**, *6*, 18782–18793. [CrossRef]
49. Hou, T.-Z.; Chen, X.; Peng, H.-J.; Huang, J.-Q.; Li, B.-Q.; Zhang, Q. Design Principles for Heteroatom-Doped Nanocarbon to Achieve Strong Anchoring of Polysulfides for Lithium-Sulfur Batteries. *Small* **2016**, *12*, 3283–3291. [CrossRef]
50. Xiao, K.; Wang, J.; Chen, Z.; Qian, Y.; Liu, Z.; Zhang, L.; Chen, X.; Liu, J.; Fan, X.; Shen, Z.X. Improving Polysulfides Adsorption and Redox Kinetics by the Co4 N Nanoparticle/N-Doped Carbon Composites for Lithium-Sulfur Batteries. *Small* **2019**, *15*, e1901454. [CrossRef]
51. Chen, M.; Zhao, S.; Jiang, S.; Huang, C.; Wang, X.; Yang, Z.; Xiang, K.; Zhang, Y. Suppressing the Polysulfide Shuttle Effect by Heteroatom-Doping for High-Performance Lithium–Sulfur Batteries. *ACS Sustain. Chem. Eng.* **2018**, *6*, 7545–7557. [CrossRef]
52. Schneider, A.; Suchomski, C.; Sommer, H.; Janek, J.; Brezesinski, T. Free-standing and binder-free highly N-doped carbon/sulfur cathodes with tailorable loading for high-areal-capacity lithium–sulfur batteries. *J. Mater. Chem. A* **2015**, *3*, 20482–20486. [CrossRef]
53. Dong, C.; Zhou, H.; Jin, B.; Gao, W.; Lang, X.; Li, J.; Jiang, Q. Enabling high-performance room-temperature sodium/sulfur batteries with few-layer 2H-MoSe2 embellished nitrogen-doped hollow carbon spheres as polysulfide barriers. *J. Mater. Chem. A* **2021**, *9*, 3451–3463. [CrossRef]
54. Fu, L.; Tang, K.; Song, K.; van Aken, P.A.; Yu, Y.; Maier, J. Nitrogen doped porous carbon fibres as anode materials for sodium ion batteries with excellent rate performance. *Nanoscale* **2014**, *6*, 1384–1389. [CrossRef] [PubMed]
55. Eng, A.Y.S.; Wang, Y.; Nguyen, D.-T.; Tee, S.Y.; Lim, C.Y.J.; Tan, X.Y.; Ng, M.-F.; Xu, J.; Seh, Z.W. Tunable Nitrogen-Doping of Sulfur Host Nanostructures for Stable and Shuttle-Free Room-Temperature Sodium–Sulfur Batteries. *Nano Lett.* **2021**, *21*, 5401–5408. [CrossRef]
56. Fu, N.; Liu, Y.; Liu, R.; Wang, X.; Yang, Z. Metal Cation-Assisted Synthesis of Amorphous B, N Co-Doped Carbon Nanotubes for Superior Sodium Storage. *Small* **2020**, *16*, e2001607. [CrossRef] [PubMed]
57. Qiu, Z.; Lin, Y.; Xin, H.; Han, P.; Li, D.; Yang, B.; Li, P.; Ullah, S.; Fan, H.; Zhu, C.; et al. Ultrahigh level nitrogen/sulfur co-doped carbon as high performance anode materials for lithium-ion batteries. *Carbon* **2018**, *126*, 85–92. [CrossRef]
58. Xia, G.; Zhang, L.; Chen, X.; Huang, Y.; Sun, D.; Fang, F.; Guo, Z.; Yu, X. Carbon hollow nanobubbles on porous carbon nanofibers: An ideal host for high-performance sodium-sulfur batteries and hydrogen storage. *Energy Storage Mater.* **2018**, *14*, 314–323. [CrossRef]
59. Li, D.; Gong, B.; Cheng, X.; Ling, F.; Zhao, L.; Yao, Y.; Ma, M.; Jiang, Y.; Shao, Y.; Rui, X.; et al. An Efficient Strategy toward Multichambered Carbon Nanoboxes with Multiple Spatial Confinement for Advanced Sodium–Sulfur Batteries. *ACS Nano* **2021**, *15*, 20607–20618. [CrossRef]
60. Zhang, B.-W.; Sheng, T.; Liu, Y.-D.; Wang, Y.-X.; Zhang, L.; Lai, W.-H.; Wang, L.; Yang, J.; Gu, Q.-F.; Chou, S.-L.; et al. Atomic cobalt as an efficient electrocatalyst in sulfur cathodes for superior room-temperature sodium-sulfur batteries. *Nat. Commun.* **2018**, *9*, 4082. [CrossRef]
61. Zhang, B.-W.; Li, S.; Yang, H.-L.; Liang, X.; Lai, W.-H.; Zhao, S.; Dong, J.; Chu, S.-Q.; Gu, Q.-F.; Liang, J.; et al. Atomically dispersed S-Fe-N4 for fast kinetics sodium-sulfur batteries via a dual function mechanism. *Cell Rep. Phys. Sci.* **2021**, *2*, 100531. [CrossRef]
62. Wang, L.; Wang, H.; Zhang, S.; Ren, N.; Wu, Y.; Wu, L.; Zhou, X.; Yao, Y.; Wu, X.; Yu, Y. Manipulating the Electronic Structure of Nickel via Alloying with Iron: Toward High-Kinetics Sulfur Cathode for Na–S Batteries. *ACS Nano* **2021**, *15*, 15218–15228. [CrossRef] [PubMed]
63. Zheng, S.; Han, P.; Han, Z.; Li, P.; Zhang, H.; Yang, J. Nano-Copper-Assisted Immobilization of Sulfur in High-Surface-Area Mesoporous Carbon Cathodes for Room Temperature Na-S Batteries. *Adv. Energy Mater.* **2014**, *4*, 1400226. [CrossRef]
64. Guo, B.; Du, W.; Yang, T.; Deng, J.; Liu, D.; Qi, Y.; Jiang, J.; Bao, S.J.; Xu, M. Nickel Hollow Spheres Concatenated by Nitrogen-Doped Carbon Fibers for Enhancing Electrochemical Kinetics of Sodium-Sulfur Batteries. *Adv. Sci.* **2020**, *7*, 1902617. [CrossRef]
65. Du, W.; Wu, Y.; Yang, T.; Guo, B.; Liu, D.; Bao, S.-J.; Xu, M. Rational construction of rGO/VO2 nanoflowers as sulfur multifunctional hosts for room temperature Na-S batteries. *Chem. Eng. J.* **2020**, *379*, 122359. [CrossRef]
66. Kumar, A.; Ghosh, A.; Roy, A.; Panda, M.R.; Forsyth, M.; MacFarlane, D.R.; Mitra, S. High-energy density room temperature sodium-sulfur battery enabled by sodium polysulfide catholyte and carbon cloth current collector decorated with MnO2 nanoarrays. *Energy Storage Mater.* **2019**, *20*, 196–202. [CrossRef]
67. Bao, W.; Shuck, C.E.; Zhang, W.; Guo, X.; Gogotsi, Y.; Wang, G. Boosting Performance of Na-S Batteries Using Sulfur-Doped Ti3C2Tx MXene Nanosheets with a Strong Affinity to Sodium Polysulfides. *ACS Nano* **2019**, *13*, 11500–11509. [CrossRef]
68. Bao, W.; Wang, R.; Qian, C.; Zhang, Z.; Wu, R.; Zhang, Y.; Liu, F.; Li, J.; Wang, G. Porous Heteroatom-Doped Ti3C2Tx MXene Microspheres Enable Strong Adsorption of Sodium Polysulfides for Long-Life Room-Temperature Sodium-Sulfur Batteries. *ACS Nano* **2021**, *15*, 16207–16217. [CrossRef] [PubMed]
69. Yang, W.; Li, X.; Li, Y.; Zhu, R.; Pang, H. Applications of Metal-Organic-Framework-Derived Carbon Materials. *Adv. Mater.* **2019**, *13*, e1804740. [CrossRef] [PubMed]
70. Ren, J.; Huang, Y.; Zhu, H.; Zhang, B.; Zhu, H.; Shen, S.; Tan, G.; Wu, F.; He, H.; Lan, S.; et al. Recent progress on MOF-derived carbon materials for energy storage. *Carbon Energy* **2020**, *2*, 176–202. [CrossRef]
71. Li, X.; Sun, Q.; Liu, J.; Xiao, B.; Li, R.; Sun, X. Tunable porous structure of metal organic framework derived carbon and the application in lithium–sulfur batteries. *J. Power Sources* **2016**, *302*, 174–179. [CrossRef]

72. Walle, M.D.; Zhang, M.; Zeng, K.; Li, Y.; Liu, Y.-N. MOFs-derived nitrogen-doped carbon interwoven with carbon nanotubes for high sulfur content lithium–sulfur batteries. *Appl. Surf. Sci.* **2019**, *497*, 143773. [CrossRef]

73. Hong, X.J.; Tang, X.Y.; Wei, Q.; Song, C.L.; Wang, S.Y.; Dong, R.F.; Cai, Y.P.; Si, L.P. Efficient Encapsulation of Small S_{2-4} Molecules in MOF-Derived Flowerlike Nitrogen-Doped Microporous Carbon Nanosheets for High-Performance Li-S Batteries. *ACS Appl. Mater. Interfaces* **2018**, *10*, 9435–9443. [CrossRef] [PubMed]

74. Chen, K.; Sun, Z.; Fang, R.; Shi, Y.; Cheng, H.-M.; Li, F. Metal-Organic Frameworks (MOFs)-Derived Nitrogen-Doped Porous Carbon Anchored on Graphene with Multifunctional Effects for Lithium-Sulfur Batteries. *Adv. Funct. Mater.* **2018**, *28*, 13–31. [CrossRef]

75. Yan, Z.; Xiao, J.; Lai, W.; Wang, L.; Gebert, F.; Wang, Y.; Gu, Q.; Liu, H.; Chou, S.L.; Liu, H.; et al. Nickel sulfide nanocrystals on nitrogen-doped porous carbon nanotubes with high-efficiency electrocatalysis for room-temperature sodium-sulfur batteries. *Nat. Commun.* **2019**, *10*, 4793. [CrossRef]

76. Luo, S.; Ruan, J.; Wang, Y.; Hu, J.; Song, Y.; Chen, M.; Wu, L. Flower-Like Interlayer-Expanded MoS_{2-x} Nanosheets Confined in Hollow Carbon Spheres with High-Efficiency Electrocatalysis Sites for Advanced Sodium-Sulfur Battery. *Small* **2021**, *17*, e2101879. [CrossRef] [PubMed]

77. Reddy, B.S.; Premasudha, M.K.-M.o; Reddy, N.S.; Ahn, H.-J.; Ahn, J.-H.; Cho, K.-K. Hydrothermal synthesis of MoS2/rGO composite as sulfur hosts for room temperature sodium-sulfur batteries and its electrochemical properties. *J. Energy Storage* **2019**, *39*, 101228. [CrossRef]

78. Yang, H.; Zhou, S.; Zhang, B.W.; Chu, S.Q.; Guo, H.; Gu, Q.F.; Liu, H.; Lei, Y.; Konstantinov, K.; Wang, Y.X.; et al. Architecting Freestanding Sulfur Cathodes for Superior Room-Temperature Na–S Batteries. *Adv. Funct. Mater.* **2021**, *31*, 2102280. [CrossRef]

79. Xiao, F.; Wang, H.; Yao, T.; Zhao, X.; Yang, X.; Yu, D.Y.W.; Rogach, A.L. MOF-Derived CoS_2/N-Doped Carbon Composite to Induce Short-Chain Sulfur Molecule Generation for Enhanced Sodium-Sulfur Battery Performance. *ACS Appl. Mater. Interfaces* **2021**, *13*, 18010–18020. [CrossRef] [PubMed]

80. Liu, H.; Pei, W.; Lai, W.H.; Yan, Z.; Yang, H.; Lei, Y.; Wang, Y.X.; Gu, Q.; Zhou, S.; Chou, S.; et al. Electrocatalyzing S Cathodes via Multisulfiphilic Sites for Superior Room-Temperature Sodium-Sulfur Batteries. *ACS Nano* **2020**, *14*, 7259–7268. [CrossRef]

81. Wang, H.; Deng, C.; Li, X.; Yan, D.; Xie, M.; Zhang, S.; Huang, B. Designing dual-defending system based on catalytic and kinetic iron Pyrite@C hybrid fibers for long-life room-temperature sodium-sulfur batteries. *Chem. Eng. J.* **2021**, *420*, 129681. [CrossRef]

82. Zhang, J.; Zhao, Y.; Guo, X.; Chen, C.; Dong, C.-L.; Liu, R.-S.; Han, C.-P.; Li, Y.; Gogotsi, Y.; Wang, G. Single platinum atoms immobilized on an MXene as an efficient catalyst for the hydrogen evolution reaction. *Nat. Catal.* **2018**, *1*, 985–992. [CrossRef]

83. Naguib, M.; Kurtoglu, M.; Presser, V.; Lu, J.; Niu, J.; Heon, M.; Hultman, L.; Gogotsi, Y.; Barsoum, M.W. Two-Dimensional Nanocrystals Produced by Exfoliation of Ti_3AlC_2. *Adv. Mater.* **2011**, *23*, 4248–4253. [CrossRef]

84. Lukatskaya, M.R.; Kota, S.; Lin, Z.; Zhao, M.-Q.; Shpigel, N.; Levi, M.D.; Halim, J.; Taberna, P.-L.; Barsoum, M.W.; Simon, P.; et al. Ultra-high-rate pseudocapacitive energy storage in two-dimensional transition metal carbides. *Nat. Energy* **2017**, *2*, 1–6. [CrossRef]

85. Song, J.; Guo, X.; Zhang, J.; Chen, Y.; Zhang, C.; Luo, L.; Wang, F.; Wang, G. Rational design of free-standing 3D porous MXene/rGO hybrid aerogels as polysulfide reservoirs for high-energy lithium–sulfur batteries. *J. Mater. Chem. A* **2019**, *7*, 6507–6513. [CrossRef]

86. Mukkabla, R.; Buchmeiser, M.R. Cathode materials for lithium–sulfur batteries based on sulfur covalently bound to a polymeric backbone. *J. Mater. Chem. A* **2020**, *8*, 5379–5394. [CrossRef]

87. Wang, Y.; Luo, Z.; Zhou, J.; Fan, X.; Zhang, J.; Jia, Y.; Chen, S.; Meng, X.; Bielawski, C.W.; Geng, J. Covalently Grafting Sulfur-Containing Polymers to Carbon Nanotubes Enhances the Electrochemical Performance of Sulfur Cathodes. *ACS Appl. Polym. Mater.* **2022**, *4*, 939–949. [CrossRef]

88. Kim, H.; Lee, J.; Ahn, H.; Kim, O.; Park, M.J. Synthesis of three-dimensionally interconnected sulfur-rich polymers for cathode materials of high-rate lithium–sulfur batteries. *Nat. Commun.* **2015**, *6*, 7278. [CrossRef] [PubMed]

89. Huang, C.J.; Cheng, J.H.; Su, W.N.; Partovi-Azar, P.; Kuo, L.Y.; Tsai, M.C.; Lin, M.H.; Jand, S.P.; Chan, T.S.; Wu, N.L.; et al. Origin of shuttle-free sulfurized polyacrylonitrile in lithium-sulfur batteries. *J. Power Sources* **2021**, *492*, 229508. [CrossRef]

90. Zhao, X.; Wang, C.; Li, Z.; Hu, X.; Razzaq, A.A.; Deng, Z. Sulfurized polyacrylonitrile for high-performance lithium sulfur batteries: Advances and prospects. *J. Mater. Chem. A* **2021**, *9*, 19282–19297. [CrossRef]

91. Frey, M.; Zenn, R.K.; Warneke, S.; Müller, K.; Hintennach, A.; Dinnebier, R.E.; Buchmeiser, M.R.; Accessible, E. Textile Fiber-Based Sulfurized Poly(acrylonitrile) as Li/S Cathode Material: Correlating Electrochemical Performance with Morphology and Structure. *ACS Energy Lett.* **2017**, *2*, 595–604. [CrossRef]

92. Kim, H.; Sadan, M.K.; Kim, C.; Jo, J.; Seong, M.; Cho, K.-K.; Kim, K.-W.; Ahn, J.-H.; Ahn, H.-J. Enhanced reversible capacity of sulfurized polyacrylonitrile cathode for room-temperature Na/S batteries by electrochemical activation. *Chem. Eng. J.* **2021**, *426*, 130787. [CrossRef]

93. Hwang, T.H.; Jung, D.S.; Kim, J.S.; Kim, B.G.; Choi, J.W. One-dimensional carbon-sulfur composite fibers for Na-S rechargeable batteries operating at room temperature. *Nano Lett.* **2013**, *13*, 4532–4538. [CrossRef]

94. Kim, I.; Kim, C.H.; Choi, S.H.; Ahn, J.-P.; Ahn, J.-H.; Kim, K.-W.; Cairns, E.J.; Ahn, H.-J. A singular flexible cathode for room temperature sodium/sulfur battery. *J. Power Sources* **2016**, *307*, 31–37. [CrossRef]

95. Li, S.; Zeng, Z.; Yang, J.; Han, Z.; Hu, W.; Wang, L.; Ma, J.; Shan, B.; Xie, J. High Performance Room Temperature Sodium–Sulfur Battery by Eutectic Acceleration in Tellurium-Doped Sulfurized Polyacrylonitrile. *ACS Appl. Energy Mater.* **2019**, *2*, 2956–2964. [CrossRef]

96. Ma, S.; Zuo, P.; Zhang, H.; Yu, Z.; Cui, C.; He, M.; Yin, G. Iodine-doped sulfurized polyacrylonitrile with enhanced electrochemical performance for room-temperature sodium/potassium sulfur batteries. *Chem. Commun.* **2019**, *55*, 5267–5270. [CrossRef] [PubMed]

97. Wang, L.; Chen, X.; Li, S.; Yang, J.; Sun, Y.; Peng, L.; Shan, B.; Xie, J. Effect of eutectic accelerator in selenium-doped sulfurized polyacrylonitrile for high performance room temperature sodium–sulfur batteries. *J. Mater. Chem. A* **2019**, *7*, 12732–12739. [CrossRef]

98. Ghosh, A.; Shukla, S.; Monisha, M.; Kumar, A.; Lochab, B.; Mitra, S. Sulfur Copolymer: A New Cathode Structure for Room-Temperature Sodium–Sulfur Batteries. *ACS Energy Lett.* **2017**, *2*, 2478–2485. [CrossRef]

99. Jana, M.; Park, J.M.; Kota, M.; Shin, K.H.; Rana, H.H.; Nakhanivej, P.; Huang, J.-Q.; Park, H.S. Surface Redox-Active Organosulfur-Tethered Carbon Nanotubes for High Power and Long Cyclability of Na–Organosulfur Hybrid Energy Storage. *ACS Energy Lett.* **2020**, *6*, 280–289. [CrossRef]

100. Yan, J.; Li, W.; Wang, R.; Feng, P.; Jiang, M.; Han, J.; Cao, S.; Zhang, Z.; Wang, K.; Jiang, K. An in Situ Prepared Covalent Sulfur–Carbon Composite Electrode for High-Performance Room-Temperature Sodium–Sulfur Batteries. *ACS Energy Lett.* **2020**, *5*, 1307–1315. [CrossRef]

101. Chen, K.; Li, H.; Xu, Y.; Liu, K.; Li, H.; Xu, X.; Qiu, X.; Liu, M. Untying thioether bond structures enabled by "voltage-scissors" for stable room temperature sodium-sulfur batteries. *Nanoscale* **2019**, *11*, 5967–5973. [CrossRef] [PubMed]

102. Fan, L.; Ma, R.; Yang, Y.; Chen, S.; Lu, B. Covalent sulfur for advanced room temperature sodium-sulfur batteries. *Nano Energy* **2016**, *28*, 304–310. [CrossRef]

103. Yu, X.; Manthiram, A. Ambient-Temperature Sodium-Sulfur Batteries with a Sodiated Nafion Membrane and a Carbon Nanofiber-Activated Carbon Composite Electrode. *Adv. Energy Mater.* **2015**, *5*, 1500350. [CrossRef]

104. Sun, J.; Lin, Y.; Sun, Z.; Zhu, S.; Amal, R.; Li, F.; Wang, D.-W. Highly cross-linked carbon sponge enables room-temperature long-life semi-liquid Na/polysulfide battery. *Mater. Today Energy* **2019**, *14*, 100342. [CrossRef]

105. Kumar, A.; Ghosh, A.; Forsyth, M.; MacFarlane, D.R.; Mitra, S. Free-Radical Catalysis and Enhancement of the Redox Kinetics for Room-Temperature Sodium–Sulfur Batteries. *ACS Energy Lett.* **2020**, *5*, 2112–2121. [CrossRef]

106. Ghosh, A.; Kumar, A.; Roy, A.; Panda, M.R.; Kar, M.; MacFarlane, D.R.; Mitra, S. Three-Dimensionally Reinforced Freestanding Cathode for High-Energy Room-Temperature Sodium-Sulfur Batteries. *ACS Appl. Mater. Interfaces* **2019**, *11*, 14101–14109. [CrossRef]

107. Kumar, A.; Ghosh, A.; Ghosh, A.; Ahuja, A.; Sengupta, A.; Forsyth, M.; MacFarlane, D.R.; Mitra, S. Sub-zero and room-temperature sodium–sulfur battery cell operations: A rational current collector, catalyst and sulphur-host design and study. *Energy Storage Mater.* **2021**, *42*, 608–617. [CrossRef]

108. Dong, C.; Zhou, H.; Liu, H.; Jin, B.; Wen, Z.; Lang, X.; Li, J.; Kim, J.; Jiang, Q. Inhibited shuttle effect by functional separator for room-temperature sodium-sulfur batteries. *J. Mater. Sci. Technol.* **2022**, *113*, 207–216. [CrossRef]

109. Saroha, R.; Heo, J.; Liu, Y.; Angulakshmi, N.; Lee, Y.; Cho, K.-K.; Ahn, H.-J.; Ahn, J.-H. V$_2$O$_3$-decorated carbon nanofibers as a robust interlayer for long-lived, high-performance, room-temperature sodium–sulfur batteries. *Chem. Eng. J.* **2022**, *431*, 134205. [CrossRef]

110. Yu, X.; Manthiram, A. Performance Enhancement and Mechanistic Studies of Room-Temperature Sodium–Sulfur Batteries with a Carbon-Coated Functional Nafion Separator and a Na$_2$S/Activated Carbon Nanofiber Cathode. *Chem. Mater.* **2016**, *28*, 896–905. [CrossRef]

111. Cengiz, E.C.; Erdol, Z.; Sakar, B.; Aslan, A.; Ata, A.; Ozturk, O.; Demir-Cakan, R. Investigation of the Effect of Using Al$_2$O$_3$–Nafion Barrier on Room-Temperature Na–S Batteries. *J. Phys. Chem. C* **2017**, *121*, 15120–15126. [CrossRef]

112. Li, H.; Zhao, M.; Jin, B.; Wen, Z.; Liu, H.K.; Jiang, Q. Mesoporous Nitrogen-Doped Carbon Nanospheres as Sulfur Matrix and a Novel Chelate-Modified Separator for High-Performance Room-Temperature Na-S Batteries. *Small* **2020**, *16*, e1907464. [CrossRef] [PubMed]

113. Yu, X.; Manthiram, A. Highly Reversible Room-Temperature Sulfur/Long-Chain Sodium Polysulfide Batteries. *J. Phys. Chem. Lett.* **2014**, *5*, 1943–1947. [CrossRef] [PubMed]

114. Saroja, A.P.V.K.; Rajamani, A.; Muthusamy, K.; Sundara, R. Repelling Polysulfides Using White Graphite Introduced Polymer Membrane as a Shielding Layer in Ambient Temperature Sodium Sulfur Battery. *Adv. Mater. Interfaces* **2019**, *6*, 1901497. [CrossRef]

115. Saroja, A.P.V.K.; Muthusamy, K.; Sundara, R. Strong Surface Bonding of Polysulfides by Teflonized Carbon Matrix for Enhanced Performance in Room Temperature Sodium-Sulfur Battery. *Adv. Mater. Interfaces* **2019**, *6*, 1801873. [CrossRef]

116. Vijaya Kumar Saroja, A.P.; Sundara, R.K.M. Core–Shell Cathode Design with Molybdenum Trioxide as the Electrocatalytic Trapping Layer for High-Energy Density Room-Temperature Sodium Sulfur Batteries. *J. Phys. Chem. C* **2020**, *124*, 7615–7623. [CrossRef]

117. Park, C.-W.; Ryu, H.-S.; Kim, K.-W.; Ahn, J.-H.; Lee, J.-Y.; Ahn, H.-J. Discharge properties of all-solid sodium–sulfur battery using poly (ethylene oxide) electrolyte. *J. Power Sources* **2007**, *165*, 450–454. [CrossRef]

118. Kim, J.-S.; Ahn, H.-J.; Kim, I.-P.; Kim, K.-W.; Ahn, J.-H.; Park, C.-W.; Ryu, H.-S. The short-term cycling properties of Na/PVdF/S battery at ambient temperature. *J. Solid State Electrochem.* **2008**, *12*, 861–865. [CrossRef]

119. Lee, D.-J.; Park, J.-W.; Hasa, I.; Sun, Y.-K.; Scrosati, B.; Hassoun, J. Alternative materials for sodium ion–sulphur batteries. *J. Mater. Chem. A* **2013**, *1*, 5256–5261. [CrossRef]

120. Wang, J.; Yang, J.; Nuli, Y.; Holze, R. Room temperature Na/S batteries with sulfur composite cathode materials. *Electrochem. Commun.* **2007**, *9*, 31–34. [CrossRef]

121. Zhao, X.-M.; Zhu, Q.; Xu, S.-D.; Chen, L.; Zuo, Z.-J.; Wang, X.-M.; Liu, S.-B.; Zhang, D. Fluoroethylene carbonate as an additive in a carbonates-based electrolyte for enhancing the specific capacity of room-temperature sodium-sulfur cell. *J. Electroanal. Chem.* **2019**, *832*, 392–398. [CrossRef]

122. Zhao, X.M.; Yan, Y.W.; Ren, X.X.; Chen, L.; Xu, S.D.; Liu, S.B.; Wang, X.M.; Zhang, D. Trimethyl Phosphate for Nonflammable Carbonate-Based Electrolytes for Safer Room-Temperature Sodium-Sulfur Batteries. *ChemElectroChem* **2019**, *6*, 1229–1234. [CrossRef]

123. Wu, J.; Liu, J.; Lu, Z.; Lin, K.; Lyu, Y.-Q.; Li, B.; Ciucci, F.; Kim, J.-K. Non-flammable electrolyte for dendrite-free sodium-sulfur battery. *Energy Storage Mater.* **2019**, *23*, 8–16. [CrossRef]

124. Kohl, M.; Borrmann, F.; Althues, H.; Kaskel, S. Hard Carbon Anodes and Novel Electrolytes for Long-Cycle-Life Room Temperature Sodium-Sulfur Full Cell Batteries. *Adv. Energy Mater.* **2016**, *6*, 1502185. [CrossRef]

125. Ren, Y.; Jiang, H.; Zhao, T.; Zeng, L.; Xiong, C. Remedies of capacity fading in room-temperature sodium-sulfur batteries. *J. Power Sources* **2018**, *396*, 304–313. [CrossRef]

126. Di Lecce, D.; Minnetti, L.; Polidoro, D.; Marangon, V.; Hassoun, J. Triglyme-based electrolyte for sodium-ion and sodium-sulfur batteries. *Ionics* **2019**, *25*, 3129–3141. [CrossRef]

127. He, J.; Bhargav, A.; Shin, W.; Manthiram, A. Stable Dendrite-Free Sodium–Sulfur Batteries Enabled by a Localized High-Concentration Electrolyte. *J. Am. Chem. Soc.* **2021**, *143*, 20241–20248. [CrossRef] [PubMed]

128. Lu, L.; Lu, Y.; Alonso, J.A.; Lopez, C.A.; Fernandez-Diaz, M.T.; Zou, B.; Sun, C. A Monolithic Solid-State Sodium-Sulfur Battery with Al-Doped $Na_{3.4}Zr_2(Si_{0.8}P_{0.2}O_4)_3$ Electrolyte. *ACS Appl. Mater. Interfaces* **2021**, *13*, 42927–42934. [CrossRef]

129. Song, S.; Duong, H.M.; Korsunsky, A.M.; Hu, N.; Lu, L. A Na+ Superionic Conductor for Room-Temperature Sodium Batteries. *Sci. Rep.* **2016**, *6*, 32330. [CrossRef]

130. Cheng, X.; Pan, J.; Zhao, Y.; Liao, M.; Peng, H. Gel Polymer Electrolytes for Electrochemical Energy Storage. *Adv. Energy Mater.* **2018**, *8*, 1702184. [CrossRef]

131. Goodenough, J.B.; Hong, H.Y.-P.; Kafalas, J.A. Fast Na^+-ion transport in skeleton structures. *Mater. Res. Bull.* **1976**, *11*, 203–220. [CrossRef]

132. Hong, H.Y.P. Crystal structures and crystal chemistry in the system $Na_{1+x}Zr_2Si_xP_{3-x}O_{12}$. *Mater. Res. Bull.* **1976**, *11*, 173–182. [CrossRef]

133. Yang, K.; Liu, D.; Qian, Z.; Jiang, D.; Wang, R. Computational Auxiliary for the Progress of Sodium-Ion Solid-State Electrolytes. *ACS Nano* **2021**, *15*, 17232–17246. [CrossRef]

134. Zhang, Q.; Cao, D.; Ma, Y.; Natan, A.; Aurora, P.; Zhu, H. Stability, and Potential for All-Solid-State Batteries. *Adv. Mater.* **2019**, *31*, e1901131. [CrossRef] [PubMed]

135. Tanibata, N.; Tsukasaki, H.; Deguchi, M.; Mori, S.; Hayashi, A.; Tatsumisago, M. Characterization of sulfur nanocomposite electrodes containing phosphorus sulfide for high-capacity all-solid-state Na/S batteries. *Solid State Ion.* **2017**, *311*, 6–13. [CrossRef]

136. Yue, J.; Han, F.; Fan, X.; Zhu, X.; Ma, Z.; Yang, J.; Wang, C. High-Performance All-Inorganic Solid-State Sodium–Sulfur Battery. *ACS Nano* **2017**, *11*, 4885–4891. [CrossRef]

137. Fan, X.; Yue, J.; Han, F.; Chen, J.; Deng, T.; Zhou, X.; Hou, S.; Wang, C. High-Performance All-Solid-State Na-S Battery Enabled by Casting-Annealing Technology. *ACS Nano* **2018**, *12*, 3360–3368. [CrossRef]

138. Ando, T.; Sakuda, A.; Tatsumisago, M.; Hayashi, A. All-solid-state sodium-sulfur battery showing full capacity with activated carbon MSP20-sulfur-Na_3SbS_4 composite. *Electrochem. Commun.* **2020**, *116*, 100860. [CrossRef]

139. Wan, H.; Weng, W.; Han, F.; Cai, L.; Wang, C.; Yao, X. Bio-inspired Nanoscaled Electronic/Ionic Conduction Networks for Room-Temperature All-Solid-State Sodium-Sulfur Battery. *Nano Today* **2020**, *33*, 100860. [CrossRef]

140. Park, K.H.; Kim, D.H.; Kwak, H.; Jung, S.H.; Lee, H.-J.; Banerjee, A.; Lee, J.H.; Jung, Y.S. Solution-derived glass-ceramic $NaI \cdot Na_3SbS_4$ superionic conductors for all-solid-state Na-ion batteries. *J. Mater. Chem. A* **2018**, *6*, 17192–17200. [CrossRef]

141. Wan, H.; Cai, L.; Yao, Y.; Weng, W.; Feng, Y.; Mwizerwa, J.P.; Liu, G.; Yu, Y.; Yao, X. Self-Formed Electronic/Ionic Conductive $Fe_3S_4@S@0.9Na_3SbS_4$ 0.1NaI Composite for High-Performance Room-Temperature All-Solid-State Sodium-Sulfur Battery. *Small* **2020**, *16*, e2001574. [CrossRef] [PubMed]

142. Ge, Z.; Li, J.; Liu, J. Enhanced electrochemical performance of all-solid-state sodium-sulfur batteries by PEO-$NaCF_3SO_3$-MIL-53(Al) solid electrolyte. *Ionics* **2020**, *26*, 1787–1795. [CrossRef]

143. Zhu, T.; Dong, X.; Liu, Y.; Wang, Y.-G.; Wang, C.; Xia, Y.-Y. An All-Solid-State Sodium–Sulfur Battery Using a Sulfur/Carbonized Polyacrylonitrile Composite Cathode. *ACS Appl. Energy Mater.* **2019**, *2*, 5263–5271. [CrossRef]

144. Judez, X.; Martinez-Ibañez, M.; Santiago, A.; Armand, M.; Zhang, H.; Li, C. Quasi-solid-state electrolytes for lithium sulfur batteries: Advances and perspectives. *J. Power Sources* **2019**, *438*, 226985. [CrossRef]

145. Kumar, D.; Suleman, M.; Hashmi, S.A. Studies on poly (vinylidene fluoride-co-hexafluoropropylene) based gel electrolyte nanocomposite for sodium–sulfur batteries. *Solid State Ion.* **2011**, *202*, 45–53. [CrossRef]

146. Kumar, D.; Hashmi, S. Ionic liquid based sodium ion conducting gel polymer electrolytes. *Solid State Ionics* **2010**, *181*, 416–423. [CrossRef]

147. Kumar, D.; Kanchan, D. Dielectric and electrochemical studies on carbonate free Na-ion conducting electrolytes for sodium-sulfur batteries. *J. Energy Storage* **2019**, *22*, 44–49. [CrossRef]

148. Hu, X.; Ni, Y.; Wang, C.; Wang, H.; Matios, E.; Chen, J.; Li, W. Facile-Processed Nanocarbon-Promoted Sulfur Cathode for Highly Stable Sodium-Sulfur Batteries. *Cell Rep. Phys. Sci.* **2020**, *1*, 100015. [CrossRef]

149. Yu, X.; Manthiram, A. Sodium-Sulfur Batteries with a Polymer-Coated NASICON-type Sodium-Ion Solid Electrolyte. *Matter* **2019**, *1*, 439–451. [CrossRef]

150. Ren, Y.; Hortance, N.; McBride, J.; Hatzell, K.B. Sodium–Sulfur Batteries Enabled by a Protected Inorganic/Organic Hybrid Solid Electrolyte. *ACS Energy Lett.* **2020**, *6*, 345–353. [CrossRef]

151. Kim, I.; Park, J.-Y.; Kim, C.H.; Park, J.-W.; Ahn, J.-P.; Ahn, J.-H.; Kim, K.-W.; Ahn, H.-J. A room temperature Na/S battery using a β″alumina solid electrolyte separator, tetraethylene glycol dimethyl ether electrolyte, and a S/C composite cathode. *J. Power Sources* **2016**, *301*, 332–337. [CrossRef]

152. Kim, I.; Park, J.-Y.; Kim, C.; Ahn, J.-P.; Ahn, J.-H.; Kim, K.-W.; Ahn, H.-J. Sodium Polysulfides during Charge/Discharge of the Room-Temperature Na/S Battery Using TEGDME Electrolyte. *J. Electrochem. Soc.* **2016**, *163*, A611–A616. [CrossRef]

153. Seh, Z.W.; Sun, J.; Sun, Y.; Cui, Y. A Highly Reversible Room-Temperature Sodium Metal Anode. *ACS Central Sci.* **2015**, *1*, 449–455. [CrossRef] [PubMed]

154. Luo, W.; Lin, C.F.; Zhao, O.; Noked, M.; Zhang, Y.; Rubloff, G.W.; Hu, L. Ultrathin Surface Coating Enables the Stable Sodium Metal Anode. *Adv. Energy Mater.* **2016**, *7*, 1601526. [CrossRef]

155. Fan, L.; Li, X. Recent advances in effective protection of sodium metal anode. *Nano Energy* **2018**, *53*, 630–642. [CrossRef]

156. Zhao, Y.; Goncharova, L.V.; Lushington, A.; Sun, Q.; Yadegari, H.; Wang, B.; Xiao, W.; Li, R.; Sun, X. Superior Stable and Long Life Sodium Metal Anodes Achieved by Atomic Layer Deposition. *Adv. Mater.* **2017**, *29*, 1606663. [CrossRef] [PubMed]

157. Zhao, Y.; Goncharova, L.V.; Zhang, Q.; Kaghazchi, P.; Sun, Q.; Lushington, A.; Wang, B.; Li, R.; Sun, X. Inorganic–Organic Coating via Molecular Layer Deposition Enables Long Life Sodium Metal Anode. *Nano Lett.* **2017**, *17*, 5653–5659. [CrossRef]

158. Kumar, V.; Eng, A.Y.S.; Wang, Y.; Nguyen, D.-T.; Ng, M.-F.; Seh, Z.W. An artificial metal-alloy interphase for high-rate and long-life sodium–sulfur batteries. *Energy Storage Mater.* **2020**, *29*, 1–8. [CrossRef]

159. Kumar, V.; Wang, Y.; Eng, A.Y.S.; Ng, M.-F.; Seh, Z.W. A Biphasic Interphase Design Enabling High Performance in Room Temperature Sodium-Sulfur Batteries. *Cell Rep. Phys. Sci.* **2020**, *1*, 100044. [CrossRef]

160. Pampel, J.; Dörfler, S.; Althues, H.; Kaskel, S. Designing room temperature sodium sulfur batteries with long cycle-life at pouch cell level. *Energy Storage Mater.* **2019**, *21*, 41–49. [CrossRef]

161. Yu, X.; Manthiram, A. Na_2S-carbon nanotube fabric electrodes for room-temperature sodium-sulfur batteries. *Chemistry* **2015**, *21*, 4233–4237. [CrossRef] [PubMed]

162. Bloi, L.M.; Pampel, J.; Dörfler, S.; Althues, H.; Kaskel, S. Sodium Sulfide Cathodes Superseding Hard Carbon Pre-sodiation for the Production and Operation of Sodium–Sulfur Batteries at Room Temperature. *Adv. Energy Mater.* **2020**, *10*, 1903245. [CrossRef]